CMIP3 21st century robust subtropical precipitation declines are mostly mid-latitude shifts

Jacob S. Scheff

A thesis submitted in partial fulfillment of the requirements for the degree of

Master of Science

University of Washington

2011

Program Authorized to Offer Degree:

Atmospheric Sciences

University of Washington

Graduate School

This is to certify that I have examined this copy of a master's thesis by

Jacob S. Scheff

and have found that it is complete and satisfactory in all respects, and that any and all revisions required by the final examining committee have been made.

Committee Members:

_____

Dargan M.W. Frierson

_____

Qiang Fu

_____

John M. Wallace

Date:_____

In presenting this thesis in partial fulfillment of the requirements for a master's degree at the University of Washington, I agree that the Library shall make its copies freely available for inspection. I further agree that extensive copying of this thesis is allowable only for scholarly purposes, consistent with "fair use" as prescribed in the U.S. Copyright Law. Any other reproduction for any purposes or by any means shall not be allowed without my written permission.

Signature _____

Date _____

University of Washington

Abstract

CMIP3 21st century robust subtropical precipitation declines are mostly mid-latitude shifts

Jacob S. Scheff

Chair of the Supervisory Committee:
Assistant Professor Dargan M.W. Frierson
Department of Atmospheric Sciences

We examine the spatially and seasonally distributed precipitation response to 21st century global warming in the CMIP3 suite of comprehensive models, focusing on the robust declines in precipitation found in the model subtropics. Current theories of this response include: circulation-independent changes directly driven by the thermodynamic water vapor increase due to warming; and changes due to dynamic shifts in the atmospheric circulation. In this study, we attempt to evaluate the relevance of these two mechanisms model-by-model. We consider each model's particular, biased, seasonally and zonally varying mean state and its spatial relationship to that model's predicted changes.

We find that almost every model has a general tendency to shift its existing mid-latitude cyclonic precipitation belts poleward in most seasons, leading to rainfall reductions on their subtropical flanks. This broad result agrees with the dynamic theory, and with a storm-track shift in particular. In addition, many of the models tend to reduce precipitation when and where actual evaporation exceeds precipitation, as predicted by the thermodynamic theory, but this is not as common nor as spatially widespread as the former tendency.

TABLE OF CONTENTS

LIST OF FIGURES

LIST OF TABLES

ACKNOWLEDGEMENTS

The author would like to thank I. Held, Q. Fu, and B. Soden for helpful conceptual conversations, as well as J. M. Wallace and K. Armour for several invaluable graphical suggestions.

1. Introduction, concepts, and general method

One of the most ubiquitous features of current models of greenhouse warming is their tendency to reduce climatological precipitation in much of the global subtropics, and to increase it throughout the high latitudes (e.g. Solomon et al. 2007). It is well known that global temperature changes of the recent Quaternary were accompanied by dramatic changes in local hydro-ecology (e.g. Hartmann 1994; Sarnthein 1978), so it is at least plausible that model projections such as these might play out in the future of the real world. From an agricultural-potential or ecological-productivity perspective, precipitation declines seem more worrisome than increases. Furthermore, recent work (Seager et al. 2007) has pointed out that, at least locally, the declines are simulated in the near term, on time scales of a few decades or less. So, it is important to understand the nature of this model behavior. Here, we explore and evaluate two prominent, independent characterizations of the 21st century precipitation responses in the World Climate Research Programme's (WCRP's) Coupled Model Intercomparison Project phase 3 (CMIP3) multi-model dataset (Meehl et al. 2007a), the standard climate-model output suite as of this writing, with a focus on the robust large-scale decreases in the subtropics.

1a. Fixed-circulation precipitation response from physics alone (dry-get-drier)

The first of these descriptions we will call the *thermodynamic* or *dry-get-drier* theory: the idea that under global warming with constant general circulation and constant relative humidity, large-scale wet areas get wetter and dry areas get drier, simply due to local moist thermodynamic and energetic constraints (e.g. Held and Soden 2006; Wetherald and Manabe 2002.)

The argument (after Held and Soden 2006) is as follows: under the above scenario,

absolute humidity will increase everywhere, following the Clausius-Clapeyron scaling, ~7% per K at Earth temperatures. With unchanged circulation, this implies that moisture transport will increase, and thus so will column-integrated moisture convergence, still at roughly 7% per K. But, climatologically, this quantity must equal precipitation (P) minus actual evaporation (E) at the surface, using the column water budget. So the pattern of climatological P-E will also amplify at 7% per K, with negative P-E ("dry") regions becoming more negative, and positive P-E ("wet") regions becoming more positive. And, since E is tied to the local surface energy supply, which is solar-dominated, E cannot change much—so the bulk of this P-E amplification will be accomplished by changes in P. Thus, roughly, P should decrease where and when $P-E < 0$; and P should increase where and when $P-E > 0$.

More precisely, if δ is the change due to 1 K local lower tropospheric warming, and we approximate the local evaporation increase by the global figure of 2% per K, then $\delta P = \delta(P-E) + \delta E \sim .07(P-E) + .02E = .07P - .05E$. So in this idealization, precipitation will decline if $P/E < 5/7$. Of course, the exact number 5/7 cannot be taken too seriously, but the principle is clear: under global warming with circulation and relative humidity held fixed, P should decline [increase] where and when P is already significantly less [more] than actual E (*dry-get-drier*).

In particular, we should expect to find robust modeled decreases in P associated with the *subtropical* ocean basins, since these are the main regions of large excesses of actual E over P, or atmospheric water export. [Such excesses also occur over certain tropical to mid-latitude well-watered land areas after the wet season (e.g. Hartmann 1994), but they clearly cannot be present in the large-scale annual mean anywhere on land, since P is the only large

water source to land.] Furthermore, within these broad subtropical dry ocean-centered areas, we should expect this mechanism to indiscriminately reduce both the tropical P equatorward of the driest zone, and the mid-latitude P poleward of the driest zone, as long as the amount of this P is significantly less than local E.

It is also worth noting, again following Held and Soden (2006), that the "dry-get-drier" argument does *not* directly apply to semi-arid or arid (water-limited) land areas in *any* latitude or season, for a number of reasons. First, we would no longer have any particular energy-constrained expectation for δE, since E here is constrained by P, not by surface energy flux. So we would be left with just the thermodynamic, $\delta(P-E) = .07(P-E)$ portion of the above argument. Since, again, E is constrained to nearly equal P here, this equation reduces to zero equals zero -- in other words, telling us what we already know: that $P–E \sim 0$ in drier land regions both at present, and in a greenhouse future, absent any circulation change. Of course, here we would really prefer a prediction for the bio-available water P=E itself, not for the much smaller local runoff that is their difference—but again, this theory does not attempt to offer one in this situation. Furthermore, the assumption of constant relative humidity is not as sound here as it is elsewhere, since the air is not adjacent to a saturated surface. Now, the above subtropical ocean-based areas of P reduction could still end up including some adjacent dry land areas, since their boundaries cannot be expected to precisely coincide with the coastline or with any particular P-E contour – but this is just a possible consequence, not a literal prediction of the theory.

Finally, Held and Soden (2006; their figures 7 and 8) provide evidence that the CMIP3 model hydrologic responses to 21st century global warming roughly follow the expectations from the above framework, at least in the multi-model mean and at planetary

scales. This seems especially true for the more basic prediction that the P-E field will amplify, $\delta(P-E) = .07(P-E)$. The δP prediction also shows planetary-scale agreement with the models, though notably the zonal-mean multi-model δP is not noticeably negative anywhere north of the Equator, in contrast with the prediction. This could possibly be ascribed to the abundance of land in the northern subtropics, combined with this theory's lack of constraint on δP in semi-arid to arid land areas, as described above.

1b. Precipitation responses due to robust changes in circulation/dynamics (tropical expansion?)

The second, distinct type of phenomena in the CMIP3 21st century output that we will consider, are the well-known robust poleward shifts of some general-circulation features, which also imply drying in the subtropics.

Yin (2005) shows that in the zonal mean, the mid-latitude storm track activity (as measured by high-pass eddy kinetic energy) shifts poleward during the 21st century in most CMIP3 models. This behavior is seen in both hemispheres, and in summer as well as in winter. Co-located with this movement of the storm tracks are physically-reassuring poleward shifts in Eady baroclinicity, high-pass momentum flux convergence, surface stress, and most notably for our purposes here, precipitation (P). In a (small) poleward shift of mid-latitude precipitation, P should increase on the existing seasonal storm track's poleward flank, and decrease on its equatorward flank, which is located in the subtropics—and so we have another mechanism working to robustly reduce P in subtropical latitudes, especially over the oceans, where the storm tracks are most pronounced. However, unlike the equal-opportunity dry-zone P reduction we expect from thermodynamics and energy, for a mid-latitude shift (in a given season) we expect a much clearer decline in the mostly mid-latitude-forced P

poleward of the driest zone, than in the mostly tropical P equatorward of the driest zone.

In addition, Lu et al. (2007) find that in almost every CMIP3 model and in both hemispheres, the boundary between the Hadley and Ferrel cells (measured as the latitude of the subtropical zero of the Eulerian mean meridional streamfunction at 500 mb) shifts O(1º) poleward with business-as-usual 21st century global warming. Presumably, this is associated with a poleward expansion of the region of zonal-mean descent associated with the driest part of the subtropics, a situation that would again be expected to suppress the subtropical flank of mid-latitude-driven P. Indeed, the latitude where zonal mean P-E switches from its subtropical negative values to its mid-latitude positive values also shifts poleward in Lu et al. (2007), and the distance it shifts in a given model is highly correlated with the distance moved by the Hadley-Ferrel boundary in that model. So, this phenomenon should also explain some of the robust P reductions in the model subtropics. Notably, it also only affects parts of the subtropics poleward of the driest zone in a given season, since the descent expands poleward at the expense of mid-latitude ascent, but does not also expand equatorward at the expense of tropical ascent.

With these similarities in mind, it could be argued that the storm track shifts and the mean-meridional-circulation shifts are two manifestations of one underlying general-circulation change, an expansion of the global tropics and retreat of the global mid-latitudes. Such a poleward-migrating trend has already been identified in satellite microwave observations of the meridional temperature structure of the tropical to mid-latitude troposphere (Fu et al. 2006) and stratosphere (Fu and Lin 2011; in press), and thus in the meridional structure of the balanced zonal wind (i.e. the subtropical jets) as well. Seidel et al. (2008) review additional subtropical to mid-latitude general circulation features that

appear to have moved poleward in recent decades.

In this view, the link between all of these phenomena would be the upper-tropospheric eddy momentum flux convergence, whose maxima are caused by the storm tracks, but whose zeroes strongly affect the location of the Hadley-Ferrel boundary around 30º latitude by a quasi-geostrophic-like balance (e.g. Vallis 2006; Walker and Schneider 2006.) The subtropical jet, in turn, would be thought of as tied to the Hadley-Ferrel boundary due to its origin in the poleward transport of angular momentum by the Hadley cell. However, we caution against immediately accepting this interpretation, since the various parts of the eddy momentum flux vs. latitude curve do not have to shift in lockstep with each other, since there are other controls on the Hadley-Ferrel boundary location besides eddy momentum flux, and since the subtropical jet itself is often a seasonally ephemeral feature. For our purposes in this study, it is enough to simply re-iterate that in any given season, both the storm-track and the Hadley mechanisms for widespread P reduction involve a *poleward* expansion of subtropical dryness at the expense of specifically mid-latitude wetness, rather than indiscriminate drying of the tropical- and mid-latitude- dominated parts of the dry subtropics.

1c. Full independence of the thermodynamic and dynamic ideas, and resulting method

Finally, it should be noted that the "dry-get-drier" moist-thermodynamics-driven precipitation response (section 1a above), and the dynamics-driven "poleward shift" (section 1b above), cannot possibly describe the same underlying phenomenon, and in fact are entirely separable conceptually. This is because dry-get-drier is the *fixed-circulation* P response to warming, while both of the poleward shift mechanisms are the P response to *circulation change*, and do not require warming.

To make this more concrete, imagine a world where global warming occurs, but the

general circulation ends up staying fixed. Among other things, this means that the Hadley cells do not expand (or weaken or strengthen), and the storm tracks do not shift. Yet, by the thermodynamic-energetic argument in section 1a, which assumes exactly this fixed-circulation setup, large portions of the deep subtropics still see declines in P.

Conversely, imagine a world where global warming does *not* occur, but the storm tracks and/or mean-descent regions shift poleward for some other reason. Globally, the absolute humidity does not increase, and the intensity of the P-E pattern does not amplify – and yet broad subtropical declines in P are observed, primarily poleward of the deepest subtropics, as the subtropical dry zones expand poleward.

These distinctions between the fixed-circulation part and the dynamics-driven part of the multi-model subtropical decline in P suggest a useful qualitative test to identify which dominate(s), illustrated in figure 1. Namely, in any model (or combination thereof), we can examine the spatial location of that model's P declines and increases, relative to that model's own biased, seasonally and zonally varying initial P-E and P climatologies. If, in a given season, the model's existing dry $P\text{-}E < 0$ zones are dominated by P declines, then perhaps these declines are directly due to moist thermodynamics as outlined in section 1a. Similarly, if the declining-P regions dominate the subtropical flanks of the initial model mid-latitude P belts, but are not robust equatorward of the P minima, then dynamical mechanism(s) involving poleward general-circulation shifts are more suspect. These are not mutually exclusive possibilities, since the climatological P and P-E patterns do not have to coincide -- but we will see that a lot of insight can still be gained from this method.

2. Model output analyzed

Throughout this study, we apply the concept of figure 1 using time series consisting of years 1981-2000 of monthly output from the CMIP3-archived climate model runs of scenario "20C3M", concatenated with years 2001-2099 from the runs of scenario "A2." Scenario 20C3M uses historical 20th century climate forcings, so we start the analysis in 1981 so as to avoid the period of strong aerosol forcing in the mid-20th century and isolate the response to greenhouse warming. Scenario A2 smoothly takes the end of 20C3M as its initial condition, and continues to strongly increase greenhouse gas levels through the 21st century, with about 800 ppmv CO2 in the atmosphere by 2099 compared to under 400 ppmv at the beginning. This "business-as-usual," high-carbon scenario is chosen for its presumably high signal-to-noise ratio for effects of greenhouse warming, with the downside that CMIP3 does not include the scenario for a few models.

However, 18 usable models still remain, and are listed in table 1. They will be used in the analyses based on the P climatology. For the analyses involving the P-E climatology, we are forced to drop one of these models because its surface latent heat fluxes, from which E has to be calculated, are not available, so this part is done using only 17 models. This is also noted in table 1. For simplicity, the heat of vaporization (for converting from latent heat flux to E) is taken to be a constant, $2.45*10^6$ J/kg. If for a given model and scenario there is more than one run archived, we take only the run numbered "1", as per convention. This prevents the models that submitted multiple runs from being over-weighted and/or having their noise artificially decreased compared to the others.

For each model and in each possible 3-month seasonal mean of the year (DJF, JFM, ..., NDJ), we compute the following fields in latitude and longitude: the 1981-2000

climatologies of P and of P-E, the difference between the 2080-2099 and 1981-2000 climatologies of P [a simple measure of the 21st century change in P], the full N=119 linear trend in P (1981-2099), and whether or not this trend is significant at 95% (using a two-tailed t-test.) We use these overlapping seasonal means because they provide a higher signal-to-noise than individual months, but do not disproportionately detect changes at certain times of the year. For change detection, we prefer this linear trend significance, since it screens out nominal changes that are not visually clear, as well as any apparent climate change effects that are actually fortuitous timing of decadal variability. However, we also compute the raw difference in ending and starting climatologies as stated above, for ease of comparison with other studies (see section 3 below.)

In the P trend significance t-test, we explicitly account for the lag-one autocorrelation r_1 of the residuals, by multiplying the variance of the trend estimator by $(1+r_1)/(1-r_1)$ during the calculation (e.g. Wilks 2006; Santer et al. 2000.) For most locations, $|r_1| < 0.2$ with no particular sign preference, but many models have sizable areas in the tropical Pacific where r_1 is of order -0.4 (not shown), which would lead to visually apparent trends being found insignificant, if it were not corrected for. Presumably, these negative tropical Pacific autocorrelations are due to the ~2 year periodicity of El Niño/La Niña in many climate models (e.g. Lin 2007). Regardless, there do not seem to be large regions with $r_1 > +0.2$ in the models examined. This suggests that a linear trend is indeed a good statistical model for these time series, and cursory visual inspection (not shown) seems to back this up.

We caution that we are not making any formal, probability-based claim about the statistical significance of our overall result in this study. This would require a more realistic null hypothesis than no change in local precipitation under global warming, and would also

require consideration of multiplicity and field significance (e.g. Wilks 2006, Livezey and Chen 1983), not to mention the dependence inherent in our use of overlapping three-month seasons. Rather, at each model gridpoint and in each season, we are simply using the two-tailed significance of the linear trend at 95% as a qualitative indicator of the presence or absence of a visually clear trend, which will then be collated into a broader picture of the time behavior of the entire P field in section 4 below.

3. Traditional multi-model ensemble analysis

We first apply the concept of figure 1 to the CMIP3 multi-model ensemble, along the lines of the studies cited in section 1 above. For a given season of the year, we would like to plot the regions of robust multi-model 21st-century P change against the multi-model mean late-20th-century climatology of P and of P-E. Only the 17 models in table 1 that archived E-related data are used, since we would like to use the same models for both comparisons (for geographic consistency.) To define "robust multi-model change" in a manner consistent with previous studies, we require the magnitude of the multi-model mean of the 21st-century change to exceed the inter-model standard deviation of the 21st-century change. In each model, we use the raw difference between late-21st-century and late-20th-century climatologies to measure this change, as described in section 2 above. These choices are all made to be consistent with the graphics in the current IPCC (Intergovernmental Panel on Climate Change) assessment report (Meehl et al. 2007b), which also analyzes CMIP3 output. We have also done these calculations using the linear trend slopes instead of the raw changes, and the results are close to identical (not shown.) The multi-model means and standard deviations of any desired quantity (e.g. 21st-century change) are computed by bilinear interpolation of each individual model's field of that quantity onto a common 0.5º x 0.5º fine grid.

Figures 2 (December-February mean) and 3 (June-August mean) show the results of this exercise. The black contours show the initial climatologies of P (top panels) and of P-E (bottom panels). The colored regions depict the locations of robust multi-model change in P (our topic of interest), and are conceptually identical to the stippling in the middle column of figure 10.9 from Meehl et al. (2007b) by construction. In fact, on inspection, the robust P

reduction regions are *geographically* almost identical as well, despite the fact that we use the A2 scenario and the IPCC / Meehl et al. figure uses the somewhat weaker A1B scenario, and despite our resulting use of fewer models than Meehl et al. [The only exception is our area of robust reduction in and near the Caribbean Sea in June-August, which is not stippled in the Meehl et al. figure.] This gives further confidence in the changes' robustness.

In both December-February (figure 2) and June-August (figure 3), the robust multi-model declines in P are strongly associated with the subtropical flanks of the multi-model mid-latitude wet zones in P, or equivalently with the mid-latitude sides of the subtropical dry zones in P (top panels.) Notably, the robust P decreases are rarely (if ever) found near or equatorward of the initial subtropical P minima, contrary to what one might guess from a cursory look at the above IPCC / Meehl et al. (2007b) figure or other similar plots that do not show the initial climatology. Also, the robust P decreases have this same distribution relative to model climatology whether the actual latitude is "subtropical" (e.g. the southern Mediterranean and adjacent Atlantic in winter) or "mid-latitude" (e.g. central Europe and the adjacent Atlantic in summer). This suggests that the poleward expansion of the subtropical dry zones due to circulation change is a dominant factor here, as outlined in section 1 above. In particular, the frequent symmetric, visually compelling placement of the robust P *increases* immediately poleward of these decreases, following the subpolar flanks of the same mid-latitude multi-model high-P zones, suggests a mid-latitude storm track shift (e.g. in the Southern Ocean and central North Atlantic in the top panels of both figures 2 and 3, and in the western North Pacific in the top panel of figure 2.)

The story told by the bottom panels of figures 2 and 3, which plot these same IPCC-type robust P change regions against the multi-model P-E climatologies, is somewhat more

complicated. Though the regions of robust P decline do leak into parts of the climatological "wet" P-E > 0 zones, they have a clear preference for the "dry" P-E < 0 zones. This suggests an additional role for the dry-get-drier direct effect of moist thermodynamics, again by the arguments from section 1. However, within the P-E < 0 zones, the robust P declines are largely restricted to their poleward rims, and they rarely occur in, near, or equatorward of the broad, deep P-E minima. Again, if dry-get-drier were the principal reason for these robust declines, then we would expect to see them distributed throughout the zones of strong negative P-E, including equatorward of the minima. Instead, the distribution suggests a dominant role for poleward expansion and dynamics, and only a secondary, constraining role for the circulation-independent direct moist thermodynamic effects.

There is one major exception to this rule of robust P decline distribution: the region in and near the low-latitude base of the multi-model North Atlantic mid-latitude P zone, which in winter (figure 2, top panel) extends from part of the eastern subtropical north Pacific up through north-central Mexico, and in summer (figure 3, top panel) moves east to cover the Caribbean and nearby areas. In both seasons, this region features robust multi-model drying, even though it is a local P maximum, not on the flank. In turn, the bottom panels of figures 2 and 3 show that this drying strongly coincides with the P-E minimum, in latitude if not in longitude. So this is the one region where the above story seems to reverse itself, though it could be argued that a poleward movement of storms might still negatively affect this area, since it is the most equatorward part of the apparent mid-latitude-driven P feature. Also, it should be cautioned that in the observed climate (e.g. Adler et al. 2003) the winter mid-latitude Atlantic P zone begins much further north and east, in the Gulf of Mexico, and so the above region of projected winter drying in figure 2 actually receives trivial winter

precipitation at present (rather than the >2 mm/day shown in the multi-model climatology.) This calls into question the immediate relevance of this wintertime P reduction claimed by Seager et al (2007). Regardless, though, this is at least some evidence that idealized-looking moist-thermodynamic-type deep subtropical P reductions can occur in the multi-model consensus, though it is unclear why this should be globally limited to a few tens of degrees longitude and one hemisphere.

The results for the remaining seasons (not shown) closely resemble those presented above for December-February and June-August, with robust multi-model declines in P still closely associated with the subtropical flanks of the main mid-latitude P belts (with a preference for P-E < 0 areas), and scarce elsewhere, with the exception of the Caribbean / Mesoamerica region.

4. Model-by-model analysis

The ensemble analysis in section 3 above gives us a useful overall picture of the model behavior, as well as a clearer interpretation of the nearly identical robust P decline regions found in the A1B output in Meehl et al. (2007b). However, one could object that key information could be lost (or at least blurred out) in the process of taking local multi-model statistics of the changes, because the models all have different geographic biases in their climatologies. That is, a gridded, geographically specific robustness measure may miss some behavior that is robust in a feature-relative sense, if the climatological feature in question (e.g. subtropical dry zone or mid-latitude wet zone) is located at different (incorrect) latitudes and/or longitudes in different models. Conversely, one might also be interested in the extent of the full inter-model diversity of feature-relative P behavior, in addition to any robust similarities. After all, each model is a distinct analog to our world, and our world will inevitably behave more like some of them than like others, in any given respect.

Therefore, we would also like to perform a model-climatology-relative analysis akin to that of section 3 on each one of the GCMs in table 1 *individually*, in addition to on the ensemble. We will refer to this as the *model-by-model* approach. Ultimately, we would like to concatenate or combine the qualitative results of these 17 or 18 individual analyses into an overall picture of the CMIP3 models' different feature-relative precipitation responses to global warming. We will pursue this complicated task in section 4b below. First, however, we will give an instructive example of one of the above-described single-model analyses making up this model-by-model view.

4a. Example of a single-model feature-relative seasonal precipitation response

We would like to make plots analogous to figures 2 and 3 for a single model: the

locations of a model's 21st-century [A2 scenario] P change in a given season, plotted against *that model's* late-20th-century climatologies of P and of P-E in that season. Obviously we can no longer use multi-model robustness as a criterion for defining 21st-century P change in this stand-alone, single-model analysis. So, we instead highlight regions in which the full 1981-2099, N=119 seasonal-P time series generated by the model has a significant linear trend at 95%, as defined and discussed in section 2 above. This is demonstrated in figure 4 for model "cccma" [see table 1], in December-February only.

We have created such plots for all 18 models and all 12 overlapping seasons; the particular case in figure 4 is chosen solely because it makes for an edifying example. Namely, significant single-model declines in P dominate the breadth of the single-model subtropical P-E < 0 regions in figure 4 (bottom panel), including the P-E minima and regions on either side meridionally, manifestly unlike the robust multi-model behavior in figure 2. Only the south Indian Ocean P-E < 0 zone is spared. This suggests a more active role for the pure thermodynamic/energetic mechanism in this model. There are also hints of storm-track-shifting behavior in the southern hemisphere response, with significant P increases lining up right across the southern mid-latitude P belt (figure 4, top panel) from significant P decreases, which are in turn somewhat separated from the above deeper-subtropical P decreases. This would be more in line with the ensemble behavior.

In any case, this model-season seems to have a richness of P response types lacking from the consensus presented in section 3. Qualitative examination of such plots for all models and all seasons suggests that the poleward-expansion / storm-track-shift type responses highlighted in the consensus are indeed ubiquitous, but that seemingly thermodynamic in-place P reductions in the various dry zones are still far from rare.

However, we clearly cannot show (18*12) different cousins of figure 4 here, so (again) we need some way of collating these model-by-model feature-relative responses into a single picture. We pursue this in the next section.

4b. Concisely classifying, recording and concatenating the single-model relative behaviors

First of all, because in any given season the major hydroclimatological features are in different locations on the latitude-longitude grid in different models (a motivating factor for this whole analysis), it is clear that we need some common criteria to define where these features are in each model, and in turn classify the locations of the respective model P responses relative to them.

It would be relatively simple to do this in the planet-wide zonal mean, because the single-model zonal-mean seasonal climatologies of P and of P-E are always very well-behaved (not shown), with a distinct three-or-four-peak structure corresponding to two mid-latitude storm tracks and one or two ITCZs, plus a minimal amount of smaller-meridional-scale noise. However, these modeled features, and/or the change patterns associated with them, are often strongly tilted when in viewed in full two-dimensions, with the eastern ends tens of degrees of latitude poleward of the western ends (see, e.g., the north Atlantic storm track or the south boundary of the southeast Pacific subtropical dry zone in figure 4, top panel.) Therefore, with zonal averaging there is a danger of assigning some part of a change region to the wrong climatological feature, and/or smearing out changes that are in the same place relative to the same feature across many latitudes, making them seem less globally robust than they are.

So, we would ideally like to define the subtropical minima, mid-latitude maxima, etc. of each model-season's initial P and P-E maps in some fully two-dimensional, holistic

fashion. There is a large literature in the computing and GIS fields on techniques that do something like this (e.g., Rana 2004, and references therein). However, application of these "surface network" methods to individual 2-D GCM climatologies of P or P-E did not yield anything useful, mainly because these fields are less spatially smooth than the topographic data such methods typically deal with; having abundant gridpoint-scale noise. (A common assumption of these methods is that their input fields have a continuous second derivative.)

Therefore, to define the locations of the various large-scale features on a given P or P-E model climatology map, we take the compromise approach of separately defining the latitudes of the features along each 1-D pole-to-pole meridian of longitude, using only the slice of the climatology along that meridian, and thus ultimately answering the questions of figure 1 separately for each meridian. More precisely, we use the zonal means over thirty-six 10º-wide pole-to-pole meridional strips (0-10ºE mean, 10-20ºE mean, ... , 350-360ºE mean), rather than the individual model grid-meridians, so as to smooth out some of the noise while preserving the ability of this technique to resolve the zonally varying latitudinal locations of the features. [A glance at figures 2, 3, or 4 shows that the features are typically tens of degrees longitude, or several of these strip-widths, in length.] This layout is illustrated in figure 5. Formally, for each model's grid, the 0-10ºE mean is defined as the mean over all grid-longitudes that fall in the interval (0º,10º], the 10-20ºE mean is defined as the mean over all grid-longitudes that fall in the interval (10º,20º], and so forth.

In this way, we solve the above 2-D feature detection problem by splitting it into thirty-six 1-D (meridional-only) feature detection problems, which are much more straightforward algorithmically. At this point, one might object that given the above-mentioned noisy nature of these fields, the precise detected feature latitudes could be highly

discontinuous between neighboring strips. Noting this, we will be sure to design our method for recording the qualitative location of the significant P changes *relative* to these detected climatological features to be insensitive to the precise latitude of the features (see section 4b(ii).)

4b(i). Hydroclimate feature definitions

Next, we need to decide how to actually define the various large-scale features, given one of the pole-to-pole single-model P or P-E seasonal-climatology profiles or transects just defined. (An example of such a strip-mean taken from figure 5 is shown in more detail as the black curve in figure 6.) It was stated above that this would be a relatively simple task, at least compared to the equivalent problem in 2-D. However, some of the strip-mean profiles are much noisier than the example in figure 6, and/or have conceptually difficult features such as large monsoon-driven tropical maxima tens of degrees latitude off of the equator, strong double ITCZs separated by extremely dry equatorial regions, and/or multiple large-scale mid-latitude maxima per hemisphere. Therefore, the general 1-D feature definition problem for these 10º zonal means is still surprisingly difficult, compared to the above-mentioned ease of coming up with criteria for the more well-behaved full-360º zonal means. After much trial and error, and extensive visual testing of the results from sets of strip-mean profiles taken from many diverse GCMs and seasons, we have determined the following long but (almost always) reasonable method for defining latitudes of the ITCZ maxim(a), subtropical minima and mid-latitude maxima of a model's climatological P or P-E on such pole-to-pole meridional profiles, and deciding when such maxima and/or minima do not exist. We will first describe this general feature definition for a meridional transect of *P* climatology; the method for P-E only has a few key differences, which will be noted at the

end.

First, all local maxima (grid-latitudes at which P is greater than at either neighboring latitude) along the profile are noted. Of course, many of these are noise or small terrain-induced features, not larger-scale maxima, and these need to be screened out in some way. This is done with a *prominence* criterion. After Rana (2004) and references therein, if we think of a continuous function z(y) as mapping a single horizontal coordinate y into vertical elevation z, like a topographic profile, then the additive *prominence* of a given local maximum y* of z(y) is defined as the minimum vertical descent one has to undergo (in either y-direction) in order to reach an even higher z-value.

For our transect P(y), where y is latitude, we can easily compute this for each local maximum y* by finding the first point to the south of y* with $P > P(y^*)$, taking the minimum P value between y* and this point, and subtracting this intervening minimum from P(y*) to obtain the necessary 'descent' needed to reach the 'higher' point. After performing the same procedure on the north side of y*, we can take the smaller of the southern and northern descents as the prominence of the maximum at y*, following the above definition of prominence as minimum vertical descent needed to reach 'higher terrain.' This is well-defined for each local maximum of P(y) except for the absolute, global maximum, to which we assign a prominence of infinity, since it has no such higher terrain to reach. Similarly, we define a 'multiplicative prominence' for each y* using the ratios, rather than the differences, between P(y*) and P at the intervening minima.

By setting empirically-determined additive and/or multiplicative prominence threshold(s) to be exceeded, we can now screen out local maxima that are too insignificant to count as large-scale features, which will help us define these features. We set a

multiplicative prominence threshold, which will be our main screening tool, at 1.75 (in other words, the additive prominence of the peak above the valley bottom defining it must be at least ¾ the valley bottom elevation, which empirically is almost always true for visually apparent mid-latitude and tropical maxima in these profiles.) This excludes most of the minor or noise peaks, except for a few in dry regions where P dips close to 0 in the noise minima. These remaining noise peaks are taken care of by setting an additional additive prominence threshold of 0.7 mm/day.

We can now define the "tropical maximum" of the transect, from which all the other feature definitions will ultimately derive, as the highest local maximum of P(y) that lies between latitudes -30º and 30º inclusive and that satisfies the multiplicative prominence threshold[1]. We then re-calculate the prominences of all the other maxima, stipulating that this tropical maximum always counts as "higher ground", even if it is in fact lower than the maximum in question (quite possible in longitudes where the ITCZ is relatively weak and there is a strong extratropical storm track.) This ensures that minima to one side of the tropical wet belt can't affect the prominence of maxima on the other side, which would occasionally lead to nonsensical results. We call the peaks that now satisfy both of the prominence thresholds the *non-trivial maxima* of P(y).

Having defined the "tropical maximum" in the preceding paragraph, we now proceed to define all the other (i.e. multiple) non-trivial ITCZ-type peaks of the P(y) transect, if there are any. Some relatively simple profiles might have none other than the above main tropical maximum, but others might have a double ITCZ (the wetter of which is the above

[1] On the very rare occasion that no such maximum exists, the entire profile is discarded and no P features are detected, on the grounds that there is no reasonable way to define a subtropical dry zone if there is no well-defined tropical wet zone.

maximum), and/or a complicated equatorial rain area with multiple strong maxima and minima (e.g. over the Maritime Continent), especially if the GCM resolution is high. So, we define other "ITCZs" as follows: the originally found tropical maximum counts as our first "ITCZ." Starting from here, we examine the first non-trivial maximum to the north. If it satisfies *any* of three criteria that make it obviously tropical in nature, we include it as an ITCZ, look for the next non-trivial maximum north, and recurse; otherwise we do not include it as an ITCZ, and we stop. These three criteria are: if the latitude of the maximum is south of 20º north; if the midpoint between this latitude and that of the previously detected ITCZ is south of 5º north; or if P(y) never goes below 5 mm/day between the two. Once we have stopped, we then go back to the original tropical maximum and repeat this whole recursive procedure heading south [exchanging the words "north" and "south" in the above criteria, of course.]

In this way, we define the set of ITCZ-type maxima of P(y) to include all non-trivial maxima equatorward of 20º latitude or of the original tropical maximum, as well as any nearby non-trivial maxima that "look tropical." This complicated definition of "tropical" is necessary because the belts around 20º-32º can host both genuine mid-latitude P maxima (e.g. south China in winter or spring, or the mid-latitude part of the South Pacific Convergence Zone) and purely ITCZ-type P maxima (e.g. north India in summer) in the models, again especially in the higher-resolution models.

We then call the northernmost of our set of ITCZ-type maxima the "north ITCZ", and the southernmost the "south ITCZ." [These will be the same point for simple profiles like that in figure 6, in which no additional ITCZs were detected beyond the original tropical maximum.] We are not interested in the behavior of model precipitation *between* these two

latitudes (e.g. in a dry cold tongue between double ITCZs over the Pacific, or in a terrain-generated P minimum in the Maritime Continent), but only *poleward* of them, since our focus is on the subtropical dry areas and their surroundings. So, for the remainder of this study we will only examine the portions of the P(y) profiles north of their respective north-ITCZ maxima, and south of their respective south-ITCZ maxima. This need to exclude equatorial cold tongues and the like from being counted as subtropical dry zones is the primary reason that we define multiple ITCZs.

Finally, we turn to the definition of the mid-latitude maxima and subtropical minima of our hydroclimatological transect. There will always be some arbitrariness in such a definition, because multiple distinct mid-latitude P (or P-E) maxima per hemisphere can sometimes exist along a given longitude line in the model climatology, and it is unclear which should be considered the main mid-latitude maximum for evaluation of the ideas in figure 1, especially if the more poleward candidate is stronger. An example of this would be the 50-60ºE strip in the northern hemisphere of figure 5. Looking at this P profile in isolation (as we are forced to; discussed above), it is hard to say whether we should equate the narrow but non-trivial P maximum south of 40ºN, or the broad P maximum centered around 60ºN, with the mid-latitude peak in figure 1. However, we press on and define a single mid-latitude maximum and subtropical minimum per hemisphere regardless, reasoning that conceptually unclear cases such as the one just discussed are relatively rare.

The south mid-latitude maximum is defined to be the most (additively) prominent non-trivial maximum south of the south ITCZ. [By the above definition of the ITCZ maxima, this has to be south of 20º south at least; otherwise it would have been classified as one.] The south subtropical minimum is then simply the point with the lowest value of P

between the south ITCZ and the south mid-latitude maximum. If in fact there is no non-trivial maximum south of the ITCZ(s), or if the putative subtropical minimum is poleward of 66.5º south, then these two southern hemisphere features are not defined for this particular longitude band. (These are not uncommon occurrences in the central Pacific in austral summer, when the model ITCZ often smoothly grades into the mid-latitude storm track as suggested by the top panel of figure 4, leaving a lack of any substantial maxima in the local southern mid-latitudes.) Finally, we define (or decline to define) the north mid-latitude maximum and north subtropical minimum in exactly the same manner, replacing "south" with "north" everywhere above. We have now completely defined the ITCZ(s), subtropical minima, and mid-latitude maxima (or lack thereof) of our arbitrary single-model-climatology transect P(y), in a way that can be easily implemented automatically. The colored vertical lines in figure 6 illustrate the locations thus defined for the example in that figure, which is again a relatively simple case (the only non-trivial maxima in the profile are the three defined large-scale maximum features themselves.)

The procedure for the (P-E)(y) profiles is almost the same, with a few important differences. First and foremost, we cannot use multiplicative prominence to screen out trivial peaks and valleys anymore, because the field is no longer positive definite—it routinely goes through zero and takes on both signs. A logarithmic measure of differences no longer makes sense. So we set only an additive prominence threshold for a peak to be called non-trivial, and set it at 1 mm/day (as opposed to 0.7 mm/day for P), since we find that the P-E profiles are often somewhat noisier than the P profiles. Because of this, we need to be a bit more careful in defining the initial tropical maximum: it will be the most prominent non-trivial maximum that is either between -23.5º and 23.5º latitude, or between -30º and 30º latitude

and at least 9 mm/day in value. Empirically, this seems to be the best resolution (for the P-E profiles) of the south and east Asian subtropical-zone difficulties described above. The procedure to identify the other ITCZ maxima is the same as for P, except that the third possible criterion is changed to P-E between the candidate peak and the previously identified ITCZ never dropping below 4 mm/day (as opposed to 5 mm/day for P), again on an empirical basis.

There is one additional empirical constraint that we place on the search for ITCZ-type peaks in the P-E transect, both the initial tropical peak and the subsequently defined ones: that if P-E at a local maximum is actually negative or near-zero, then the plain *precipitation* P at the P-E maximum must exceed a certain "believability" value for it to be considered a non-trivial maximum for ITCZ purposes. More precisely, P must exceed 1.5 mm/day at land-influenced latitudes (strip-mean gridcell land fraction > 0.2), or 0.5 mm/day at ocean-dominated latitudes (mean land fraction < 0.2), for a local maximum in P-E whose value is less than +0.05 mm/day to be considered non-trivial, even if it has sufficient prominence. This is because meridional changes in E that are solely due to the character of the underlying surface, and are not a consequence of meteorological conditions, can single-handedly produce pronounced low-latitude peaks in P-E in low-P regions where E usually equals or exceeds P.

For example, the eastern part of the wintertime Sahara Desert appears as a clear meridional *maximum* in climatological P-E in some models. Of course, this is because both P and E in the desert, and thus P-E, are basically zero, while both the Mediterranean Sea immediately to the north and the dry-season well-watered Sudanian zone to the south have significantly negative P-E. Since we clearly don't want to call the Sahara an ITCZ, we

require near-zero or negative maxima in P-E to actually have ample P, as detailed above, to be considered non-trivial in the ITCZ searches. [Some weak stretches of the genuine model oceanic ITCZs do have P-E < 0, so we can't simply dismiss non-positive P-E maxima out of hand.] Similar examples of spurious P-E "ITCZs" occur over the model oceans, too, as a result of surface temperature gradients leading to E gradients in non-precipitating regions (for example, a sharp P-E maximum is often associated with the east Pacific cold tongue in models that don't precipitate in the area), and this step screens those out as well.

Finally, given these ITCZ maxima in (P-E)(y), the definitions of the mid-latitude maxima and subtropical minima are exactly analogous to those for P(y). The only difference is that (again) there is no multiplicative prominence threshold for deciding which maxima are non-trivial, only the 1 mm/day additive prominence threshold. (The above spurious-maximum issue turns out not to be a problem in the relatively wet, cool mid-latitudes, so we don't impose a constraint of the type just discussed.)

So, the large-scale features of each initial climatological P and P-E transect in each season of each model are now all defined in a consistent manner. Again, these automatable definitions seem complicated, but they generally test extremely well against human visual determination across a range of models, seasons and longitudes, unlike simpler criteria that run into one of the above pitfalls. [Furthermore, we will see in section 4c below that the interesting model P responses to global warming are generally located outside of the single region (south and east Asia) that accounts for most of the difficulties encountered by these definitions.]

4b(ii). Recording and tabulating the locations of the P change relative to these features

Having just defined the large-scale late 20th century model hydroclimate (P and P-E)

features of a pole-to-pole 10º-longitude-mean transect, we would now like to notate the meridional locations of the significant 21st-century *changes* in strip-mean model P relative to these features, in a way that will be easy to synoptically combine across many models, longitudes and/or seasons into a single dataset that can be viewed compactly. Furthermore, as mentioned above, this recording convention must be fairly insensitive to the precise latitudes of the climate features, which can be rather arbitrary and 'jumpy' from strip to strip if the extrema are broad and diffuse (e.g., the south subtropical minimum in the example P profile in figure 6 would move five or ten degrees equatorward under small changes in certain P values.)

With these goals in mind, we proceed as follows. As in the previous subsection, we will first fully explain the process for the analysis relative to initial climatological P, which is slightly simpler, and then note how the analysis relative to P-E differs.

First, we discard the small minority of model-season-transect-hemispheres for which the mid-latitude maximum and subtropical minimum in P climate were not defined, since clearly the questions posed in section 1 and figure 1 cannot be answered if we do not have these features. We then conceptually split the remaining profiles at the latitudes of the features, thus decomposing each half-transect into three roughly monotonic segments: the geographically appropriate flank of the ITCZ, the subtropical flank of the storm track, and the subpolar/polar flank of the storm track. This decomposition can be pictured in both hemispheres with the aid of the example profile in figure 6.

On each of these three profile-segments, we now note the overall minimum and maximum P values. Normally, these are the values at the segment end latitudes (i.e. the defined large-scale features) by design; the only exception being the minimum P value of the

polar flank of the storm track, which might not quite be attained at the pole itself (see, e.g., figure 6 just south of 80ºN.) For a given segment, we proceed to compute five equally spaced intermediate values of P, at P = 1/6, 2/6, 3/6, 4/6, and 5/6 of the way from the minimum P value of that segment up to the maximum. These are plotted in figure 6 as sets of horizontal black lines that span the latitude range of each segment. In this way, we divide each profile segment into six equal bins *in the P (dependent-variable) direction*, à la Lebesgue integration, and classify each point of the initial profile according to which P-bin of which segment its P value belongs to (e.g. which rectangle in figure 6 it lies in): 0 to 1/6 of the way up, 1/6 to 2/6 of the way up, ..., or 5/6 to 6/6 of the way up from the segment's P minimum to its P maximum. The minimum and maximum points themselves are put into their own mini-bins at the top and bottom, for eight P-bins total per segment.

Then, for each individual P-bin (of each segment of each 10º-longitude-mean transect [on which the necessary large-scale features were defined] of each model's initial P climatology in each season), we record three key quantities. These are (1) the total number of points of the transect (i.e. grid-latitudes) in the bin, (2) the number of those grid-latitudes for which the model's 21st-century trend of the 10º-longitude-mean seasonal P at that latitude is 95%-significant (see section 2) and negative, and (3) the number of those grid-latitudes for which this same local trend is 95%-significant and positive. Normalizing (2) and (3) by (1) then gives the *fraction of points drying* **d**, and the *fraction of points wetting* **w**, of this P-bin. If there in fact are no points in this P-bin for this particular profile (e.g. the bin 2/6 to 3/6 of the way up from the north subtropical minimum to the ITCZ in the example of figure 6), then **d** and **w** are left blank, with a missing-value placeholder.

These values **d** and **w** are meaningful indices of the existence and sign of the climate-

feature-relative precipitation responses, that can then be tabulated and averaged across the same P-bin "coordinate" (e.g. "2/6 to 3/6 of the way up from the north subtropical minimum to the ITCZ") of many longitude strips, models, and/or seasons to get an overall view. Figure 7 shows **d** and **w** plotted (in percent form) for each bin and segment of the example transect in figure 6. Figure 8, akin to the top panel of figure 4 but for the model-season featured in figures 5-7, charts the global regions of pointwise significant P change for this model and season with the figure-6 transect highlighted, so that the correspondence of the wetting and drying parts of the transect with the indices in figure 7 can be noted.

A few notes about the interpretation of the P-bin "coordinate" system featured in figure 7 are now in order. First of all, because the inter-feature P(y) profile segments are not always monotonic (due to the presence of noise and minor peaks), a single P-bin may not contain latitudes that are all adjacent to each other – and so the ordinates *within* each rectangle of a plot like figure 7 can't be interpreted in a purely geographic sense. This can be seen in (for example) the top bin of the south-subtropical-minimum-to-ITCZ segment in figure 6, which contains two disconnected latitude bands, separated by latitudes that get classified into the bin below. However, this disadvantage of the Lebesgue-style vertical bin system is overshadowed by the advantages of its low sensitivity to the exact latitudes of the features, and its high sensitivity to the precipitation (or P-E) structure, which (unlike the latitudes themselves) is the relevant variable to the theories discussed in section 1.

For example, if small perturbations to the profile in figure 6 were to move the formally defined south subtropical minimum equatorward to, say, 35ºS, the only effect on the classification of the latitudes would be to move some latitudes currently in the driest bin of the ITCZ-flank segment, into the driest bin of the storm-track-flank segment – two lines

down in figure 7. In contrast, a classification based on equal bins of latitude itself would have altered the assignments of numerous latitudes, ranging from 60ºS nearly to the equator, in response to such a small P perturbation. Therefore, the P-bin system is less sensitive to arbitrary feature definitions, as desired above. Similarly, if we consider the classification of the points around 30ºS (just equatorward of the broad subtropical minimum) in figure 6, our system places them conceptually "close" to the subtropical minimum, as thinking about the ideas in section 1 demands, rather than nearly halfway to the ITCZ, as a latitude-based classification would imply. (The situation around 70ºN is similar.) This is the main motivation for the P-bin (or P-E-bin) system for recording the locations of the P responses relative to the defined hydroclimate features.

We would also like to make a few comments about the nature of the precipitation response indices **d** and **w**. First, it can be seen in figure 7 that **d**, the percentage of the bin's latitude points that get drier (P-wise) with global warming, and **w**, the percentage of the bin's points that get wetter with global warming, frequently do not add to unity. This is fine, because it is quite possible and common for a local 21st-century model P trend to *not* be significant at 95% (e.g. all the white space in figures 4 and 8), in which case that particular latitude does not add anything to **d** nor **w** for that bin, and so $\mathbf{d} + \mathbf{w} < 1$.

Second, for an individual profile like that featured in figures 6 and 7, we can see that both **d** and **w** are almost always either 0 or unity; they rarely take on intermediate values. This is also to be expected, because figure 8 demonstrates that the individual bins of each strip are usually going to be smaller than the large-scale regions of P change (or non-change), and will often be enveloped entirely by one of them. Thus, by far the most common values of the pair (**d**,**w**) for an individual bin will be (0,0) [e.g. if the bin is solidly in a white region

in figure 8], (1,0) [a red region], or (0,1) [a blue region]. Fractional values would then denote "undecided" bins situated along the margins of or boundaries between the significant P change regions, or in locations with a scattering of significant P change, and would be somewhat rarer. So, if we average together the equivalents of figure 7 for many profiles (as we will do in section 4c shortly), we can think of the average **d** at each bin "coordinate" as the *fraction of profiles for which that feature-relative "location" dries in P*, and similar for the average **w**, since the average of a list of zeroes and ones is the fraction of its entries that are ones.

The procedure for recording the locations of the significant P changes in each strip relative to the P-E climatology features, as opposed to the P climatology features, is almost identical, except for one very important difference. Namely, if any of the individual feature-to-feature or pole-to-feature P-E profile segments takes on both positive (> +0.05 mm/day) and negative (< -0.05 mm/day) values of P-E, we declare both +0.05 mm/day and -0.05 mm/day to be P-E bin boundaries (analogs to the horizontal black lines in figure 6), and name the resulting bin the "P=E" bin. We then bound the segment's remaining P-E bins at 1/4, 2/4, and 3/4 of the way from +0.05 mm/day up to the P-E maximum, and at 1/4, 2/4, and 3/4 of the way from the P-E minimum up to -0.05 mm/day, for nine interior bins total of varying width. For segments that retain the same sign throughout, we simply use 1/4, 2/4 and 3/4 of the way from the P-E minimum up to the P-E maximum, for four equal interior bins.[2] Of course, this is all done because the *sign* of climatological P-E is important for evaluating the relevance of the dry-get-drier / thermodynamic-energetic theory for robust subtropical P decline discussed in section 1a, and because P-E ~ 0 has its own physical

[2] On the rare occasion that one of the segment's global extrema is actually in the interval [-0.05 mm/day, 0.05

interpretation, separate from P-E < 0 or P-E > 0, when the underlying surface is land (again, see section 1a, and the caution at the end of section 4b(ii) above.)

This need to separate the P-E < 0 and P-E > 0 parts of each feature-to-feature segment of the P-E profiles is another key reason why we bin each segment according to hydroclimate value (instead of latitude) for classification purposes. If a noisy profile segment were to cross the P-E ~ 0 line several times on the way from, say, a subtropical P-E negative minimum up to an ITCZ-type P-E positive maximum, we would not be able to designate a particular *latitude* to separate the "dry" and "wet" parts of the segment for the purposes of section 1a. However, if we classify the latitudes by their P-E value, this is not a problem. In this way, the fact that the ordering of the bins does not always reflect the spatial ordering of the profile points, pointed out as a disadvantage for the P profiles, is actually a great advantage for usefully defining the parts of the P-E profiles.

Ordinarily, the subtropical minimum of each P-E half-profile is negative, and the other features (as well as all points poleward of the mid-latitude maximum) are positive, so that only the ITCZ flank and the subtropical flank of the mid-latitude maximum are split at P-E ~ 0 in this way. This is assumed the default configuration in the plots to be shown in section 4c. Of course, parts of some profiles will behave differently on occasion - so these parts will be tabulated and plotted separately from the above default. Specifically, the subtropical minimum may be positive (in a relatively wet part of the summer subtropics), or perhaps the ITCZ maximum may be negative (in a weak oceanic ITCZ situation). [The mid-latitude maximum in P-E is never found to be negative for any profile.] Independently, parts of the subpolar flank of the mid-latitude maximum may have negative P-E (if a warm ocean

---

mm/day], then we still treat this interval separately, so there will be five interior bins.

current, such as the North Atlantic Current, intersects this flank, for example.) All of these would require different P-E bin configurations than the default, with different interpretations - so again, each alternative P-E structure will have **d** and **w** values tabulated, averaged and plotted separately in the following section (for those parts of the profile where the binning differs from the default.)

4c. Displaying the family of recorded single-model feature-relative P responses to global warming

We now display the results of averaging and/or overlaying many plots of the type shown in figure 7, across many different 10º-longitude strips, overlapping 3-month seasons, and/or GCMs, to paint an overall picture of the models' various P responses to 21st-century global warming relative to their respective P and P-E late 20th century climatologies. These results will largely parallel what we found for the simple multi-model ensemble analysis in section 3, confirming the relevance of those results in spite of differing model biases.

Figures 9 and 10 show every GCM's **d** (fraction of points in bin drying) and **w** (fraction of points in bin wetting) profiles with respect to the meridional P features and P bins (as in figure 7), averaged bin-wise over all longitude strips for which the features in question were defined, for December-February (figure 9) and June-August (figure 10). As discussed above, these values can be roughly thought of as the *fraction of longitudes model-worldwide that get significantly drier or wetter (in P)* in response to global warming, for a particular feature-relative meridional location, model, and season. Figure 11 shows the bin-wise mean of all twelve plots of this type (December-February [figure 9], January-March, ... , November-January.)

For almost every P-bin from pole to pole, in every season and in the average over all

seasons, most models have some longitude strips that get wetter, and likewise some that get drier - that is, very few of the longitudinally-averaged single-model **d** or **w** values in figures 9 - 11 are exactly zero.

However, there are many bins in which one behavior robustly dominates over the other. In figure 11 (the average over all seasons), widespread drying is clearly more common than widespread wetting *between the subtropical minima and the mid-latitude maxima* (i.e. on the subtropical flanks of the mid-latitude P belts), dramatically so in the southern hemisphere. In great contrast, at the subtropical P minima themselves, and in the first (driest) few P-bins on their equatorward sides, the typical extents of drying and wetting are comparable. That is, all models do decrease deep-subtropical P in some longitudes, but they also all *increase* deep-subtropical P in about the same number of other longitudes [for which the P features were defined], so there's no clear *preference* toward drying.

This pattern, and the nearly identical behavior found in the individual-season plots (e.g. figures 9 - 10), strongly suggests a key role for the circulation-change-driven *poleward expansion* of the subtropical dry zones (section 1b), rather than their thermodynamically driven, energetically constrained in-place intensification, in the above 21st-century model P reductions. This pattern also closely parallels what we found in the ensemble analysis of section 3 (e.g. the top panels of figures 2 and 3): no clear P reductions in or equatorward of the subtropical P minima, in contrast to clear P reductions poleward of the minima, which led us to the same conclusion.

Now we display some model-by-model results analogous to the *bottom* panels of figures 2 and 3: overall views of the models' significant P trend locations relative to the features of the respective late 20th century P-E climatologies. Figures 12-13 (northern

hemisphere) and 14-15 (southern hemisphere) plot the same type of all-appropriate-longitudes, all-12-seasons averages of **d** and **w** for each GCM as in figure 11, except that now **d** and **w** have been computed for (and averaged/combined along) the P-E bins/features, instead of the P bins/features.

In the left panel of figure 12 or 13 (the means over the northern-hemisphere default-configured profile segments), we can see that the drying response strongly dominates the wetting response in only one (pseudo-)meridional band: poleward of the (negative) subtropical P-E minimum, but not so far toward the mid-latitude maximum that P-E has gone positive. This, too, is closely analogous to the corresponding robust ensemble response we described in section 3, and again suggests that the thermodynamic mechanism is probably not the main reason for the 'victory' of the P reductions (otherwise they would dominate equatorward of the P-E minimum as well, nearly to the other zero line), but may play a key constraining role on the poleward side.

The right panels of figures 12 and 13, which display the **d** and **w** statistics for the various non-default types of profile segments described at the end of section 4b above, add to this impression that the sign of P-E still matters somewhat. Figure 12 shows that where the subtropical P-E minimum is actually positive, a P wetting response strongly dominates in the subtropics, in stark contrast to the above default case. Similarly, figure 13 shows that where various profile segments that normally have P-E > 0 instead have P-E < 0, P drying responses become much more common than in the corresponding default cases.

Figures 14 and 15 (like figures 12 and 13, but for the southern hemisphere, with the South Pole at the top) are similar, except that the inner-mid-latitude P=E bin doesn't seem to constrain the region of robust P drying the way it does in the northern hemisphere, and the

dominance of P drying poleward of the subtropical P-E minimum is even more pronounced than in the northern hemisphere. In other words, this looks like more of a *pure* dynamical, poleward-expansion type response. This is a bit unlike the pattern in the traditional ensemble in section 3, where there seems to be more of a preference for the P drying to lie equatorward of P=E.

In the interest of brevity, we do not show the equivalents of figures 9-10 (individual seasons) for the P-E feature-relative responses, but they are broadly similar to figures 12-15 above. For the default feature configuration, deeper-subtropical P reductions are somewhat more prevalent than in figures 12-13 during northern spring and summer. Similarly, in some southern seasons, the region of dominant P declines is more constrained by the inner-mid-latitude P=E line than it is in figures 14-15.

Finally, we show the feature-relative profiles of **d** and **w** averaged not over all longitude strips of a given model, but over all models [that have the features defined] for a given longitude strip. Figure 16 shows the multi-model average of **d** as a function of P climate profile segment, bin, and (actual) longitude strip, for December-February, and figure 17 shows the same for **w**. As discussed more generally in section 4b(ii) above, these can be interpreted as the *fraction of models that significantly reduce/increase P* in this season in this P-feature-relative "location."

Figures 16 and 17 show that the above-noted tendency for the models to primarily reduce P poleward (and not equatorward) of the model subtropical P minima is not zonally uniform, at least in December-February. Instead, it is very pronounced, even more than figure 9 suggests, in the Euro-Mediterranean (~350º-50ºE), northwest Pacific (~130º-200ºE), southeast Atlantic (~0º-30ºE), south Indian Ocean (~90º-150ºE), and southeast Pacific

(~230º-290ºE) regions, while it is absent or even reversed over much of the American and west Atlantic sectors, especially in the northern hemisphere. The feature-relative P reductions in these latter areas are less robust, but look more like indiscriminate subtropical drying, than in the former areas. This view usefully complements the analogous message from the top panel of figure 2, in the traditional ensemble analysis.

Figures 18 and 19, which are exactly analogous to figures 16 and 17 but for June-August, show this zonal asymmetry even more dramatically: the American-sector northern subtropics (~240-320ºE), and the south Atlantic subtropics (~330º-10ºE) to a lesser extent, frequently feature dominant P drying everywhere from the model ITCZ maxima in P nearly to the model mid-latitude maxima in P. In contrast, the north Atlantic, and the remainder of the Southern Ocean, behave like the means in figure 10, with far more robust P reductions poleward of the subtropical minima than equatorward. This shows that the robustness of our poleward-shift, "dynamic" drying pattern owes much to its dominance of longitude space, in addition to the dominance of model space shown in figures 9-11.

In the interest of brevity, we again omit the (P-E)-climatology-based equivalents of figures 16-19; they tell much the same story that the P-based figures did.

5. Summary and discussion

In section 1 of this study, we asked a basic, and to our knowledge unanswered, question about the well-known robust tendency of dynamical Earth climate models to reduce precipitation (P) in the subtropics in response to global warming: to what extent does this pattern appear to be a consequence of the well-known poleward shifts of the models' general circulation features, compared to the fixed-circulation, fixed-relative-humidity energetic requirement that the subtropical P be reduced? We proposed to contribute to the resolution of this dilemma by explicitly documenting the locations of the significant model P reductions *relative to the model climatologies* of P and of P-E (precipitation minus evaporation), and comparing these climate-relative locations to the theoretical expectations from each of these two strictly and necessarily distinct mechanisms.

Two very different approaches to this task, a simple multi-model ensemble diagnostic taken from the existing literature (section 3) and a novel system for uniformly recording the geography of each individual model's P changes relative to the geography of that model's large-scale hydroclimate features (section 4), have now suggested essentially the same answer to the above question. Namely, in both of these views, the robust model P declines dominate the subtropical flanks of the model mid-latitude storm tracks, especially the drier portions, but do not dominate the central nor equatorward parts of the model dry subtropics. This strongly suggests that they mostly consist of the hydrologic consequences of known poleward shifts in the model storm tracks and/or Eulerian-mean subtropical descent belts, and are not primarily made up of the 'dry-get-drier' general moist thermodynamic response to warming as often suggested in the literature. However, both methods also support localized exceptions to these rules, especially in the subtropical northern-hemisphere

Americas and surrounding seas.

One might question to what extent these results are relevant to real-world future precipitation change, given that many (if not all) of the CMIP3 models are imperfect at best at simulating the actual present-day low-latitude precipitation distribution (e.g. Solomon et al. 2007). For the purposes of this study, we prefer to think of our 17 or 18 GCMs not as direct projections of real-world change, but rather as analog or "toy" climate systems, incorrigibly different from our Earth, but which like our Earth obey the basic physical assumptions of the both the thermodynamic and dynamic mechanisms for subtropical P reduction: the Clausius-Clapeyron equation, the tendency for relative humidities to stay near-constant under climate change (e.g. Held and Soden 2006), the presence of baroclinic storm tracks and mean meridional circulations roughly analogous to Earth's, the action of rotating stratified baroclinic dynamics in a spherical atmosphere, the generation (suppression) of precipitation by ascent (descent), and so forth. If the P reductions are supposed to follow only from these basic properties, then it seems reasonable to suppose that even the models with very biased P climatologies might experience both types of reductions, *relative to the geography of those biased climatologies*, and therefore have something to tell us about the possible hydroclimate futures of our own world.

Finally, one might object that hydroclimate, both oceanic and terrestrial, is as much a function of evaporation as it is of precipitation, especially in the warm climates that we are concerned with in this study, and that we have ignored the former in favor of analyzing the latter. We fully acknowledge this point, and defend ourselves only by positing that the evaporation responses are mostly insolation-constrained and are thus expected to be relatively featureless compared to the precipitation responses, as discussed in section 1a

above after Held and Soden (2006). However, we fully intend to contribute to the analysis of the evaporative climate response to global temperature change in future work.

REFERENCES

Adler, R. F., and co-authors, 2003: The version-2 Global Precipitation Climatology Project (GPCP) monthly precipitation analysis (1979–present). *J. Hydrometeor.* **4**, 1147–1167.

Fu, Q., C.M. Johanson, J.M. Wallace, and T. Reichler, 2006: Enhanced mid-latitude tropospheric warming in satellite measurements. *Science* **312**, 1179.

Fu, Q., and P. Lin, 2011: Poleward shift of subtropical jets inferred from satellite-observed lower stratospheric temperatures. *J. Clim.* (in press).

Hartmann, D., 1994: *Global Physical Climatology*. Academic Press.

Held, I., and B. Soden, 2006: Robust responses of the hydrological cycle to global warming. *J. Clim.* **19**, 5686-99.

Lin, J. L., 2007: Interdecadal variability of ENSO in 21 IPCC AR4 coupled GCMs. *Geophys. Res. Lett.* **34**, L12702.

Livezey, R. E., and W. Y. Chen, 1983: Statistical field significance and its determination by Monte Carlo techniques. *Mon. Wea. Rev.* **111**, 46–59.

Lu, J., G.A. Vecchi, and T.J. Reichler, 2007: Expansion of the Hadley cell under global warming. *Geophys. Res. Lett.* **34**, L06805.

Meehl, G. A., C. Covey, T. Delworth, M. Latif, B. McAvaney, J. F. B. Mitchell, R. J. Stouffer, and K. E. Taylor, 2007a: The WCRP CMIP3 multi-model dataset: A new era in climate change research. *Bull. Amer. Meteor. Soc.* **88**, 1383-1394.

Meehl, G.A., and co-authors, 2007b: Global climate projections. In: *Climate Change 2007: The Physical Science Basis. Contribution of Working Group I to the Fourth Assessment Report of the Intergovernmental Panel on Climate Change* [Solomon, S., D. Qin, M. Manning, Z. Chen, M. Marquis, K.B. Averyt, M. Tignor and H.L. Miller (eds.)]. Cambridge University Press.

Rana, S. (ed.), 2004: *Topological Data Structures for Surfaces: An Introduction to Geographical Information Science*. Wiley.

Santer, B.D, T.M.L. Wigley, J.S. Boyle, D.J. Gaffen, J.J. Hnilo, D. Nychka, D.E. Parker, and K.E. Taylor, 2000: Statistical significance of trends and trend differences in layer-average atmospheric temperature time series. *J. Geophys. Res.* **105**, 7337-7356.

Sarnthein, M., 1978: Sand deserts during glacial maximum and climatic optimum. *Nature* **272**, 43-46.

Seager, R., and co-authors, 2007: Model projections of an imminent transition to a more arid climate in southwestern North America. *Science* **316**, 1181-1184.

Seidel, D.J., Q. Fu, W.J. Randel, and T.J. Reichler, 2008: Widening of the tropical belt in a changing climate. *Nature Geosci.* **1**, 21-24.

Solomon, S., and co-authors, 2007: Technical summary. In: *Climate Change 2007: The Physical Science Basis. Contribution of Working Group I to the Fourth Assessment Report of the Intergovernmental Panel on Climate Change* [Solomon, S., D. Qin, M. Manning, Z.

Chen, M. Marquis, K.B. Averyt, M. Tignor and H.L. Miller (eds.)]. Cambridge University Press.

Vallis, G.K. (2006). *Atmospheric and Oceanic Fluid Dynamics*. Cambridge University Press.

Walker, C. C., and T. Schneider, 2006: Eddy influences on Hadley circulations: simulations with an idealized GCM. *J. Atmos. Sci.* **63**, 3333-3350.

Wetherald, R.T., and S. Manabe, 2002: Simulation of hydrologic changes associated with global warming. *J. Geophys. Res.* **107**, 4379.

Wilks, D.S., 2006: *Statistical Methods in the Atmospheric Sciences, Second Edition*. Academic Press.

Yin, J., 2005: A consistent poleward shift of the storm tracks in simulations of 21st century climate. *Geophys. Res. Lett.* **32**, L18701.

Appendix: Tables

Table 1. The 18 WCRP CMIP3 (Meehl et al. 2007a) climate models with output from scenarios 20C3M and A2 analyzed in this study. *: this model did not archive surface latent heat fluxes or evaporation, and therefore was not used in any of the analyses requiring evaporation output.

Model name and origin	Abbreviation used in this study
BCCR-BCM2.0, Norway	bccr
CCSM3, USA	ccsm3_0
CGCM3.1(T47), Canada [CCCMA]	cccma
CNRM-CM3, France	cnrm
CSIRO-Mk3.0, Australia	csiro3_0
CSIRO-Mk3.5, Australia	csiro3_5
ECHAM5/MPI-OM, Germany	mpi
ECHO-G, Germany/Korea [MIUB]	miub
GFDL-CM2.0, USA	gfdl2_0
GFDL-CM2.1*, USA	gfdl2_1
INGV-SXG, Italy	ingv
INM-CM3.0, Russia	inm
IPSL-CM4, France	ipsl
MIROC3.2(medres), Japan	miroc
MRI-CGCM2.3.2, Japan	mri
PCM, USA	pcm
UKMO-HadCM3, UK	hadcm3
UKMO-HadGEM1, UK	hadgem1

Appendix: Figure Captions

Figure 1. Conceptual model for inferring the dynamic vs. thermodynamic nature of simulated subtropical precipitation reductions. The simulated late 20th century precipitation climatology for a particular model, time of year, and longitude band is plotted, but we could ask this question for any model, at any time of year, and in any longitude where there is a distinct subtropical minimum and mid-latitude maximum. We could have also used the climatology of precipitation minus evaporation.

Figure 2. All data December-February only. Black contours: 1981-2000 multi-model climatological precipitation (top panel; 1, 2, 5 mm/day lightest to boldest) and precipitation minus evaporation (bottom panel; -2.5, -0.5 mm/day light; +0.5, +2.5 mm/day bold; 0 contour not shown). Colors: locations of robust multi-model 21st century precipitation decreases (red) and increases (blue); colors are reproduced in both panels.

Figure 3. As figure 2, but all data June-August only. Black contours: 1981-2000 multi-model climatological precipitation (top panel; 1, 2, 5 mm/day lightest to boldest) and precipitation minus evaporation (bottom panel; -2.5, -0.5 mm/day light; +0.5, +2.5 mm/day bold; 0 contour not shown). Colors: locations of robust multi-model 21st century precipitation decreases (red) and increases (blue); colors are reproduced in both panels.

Figure 4. All data December-February only, and for the single GCM "cccma" only. Black contours: 1981-2000 single-model climatological precipitation (top panel; 1, 2, 5 mm/day lightest to boldest) and precipitation minus evaporation (bottom panel; -2.5, -0.5 mm/day light; +0.5, +2.5 mm/day bold; 0 contour not shown). Colors: locations of 95%-significant single-model precipitation decreases (red) and increases (blue) using the 1981-2099 linear trends; colors are reproduced in both panels.

Figure 5. Example of the slicing of a single-GCM precipitation climatology (black contours) into thirty-six 10º-longitude-wide strips over which zonal means will be taken; the latitudes of the ITCZ maxim(a), subtropical minima and mid-latitude maxima can now be separately identified for each strip that possesses them, using the criteria of section 4b(i). The example climatology shown is that of model "hadgem1", 1981-2000, for the March-May season.

Figure 6. Black curve: zonal-average precipitation vs. latitude profile for the 290º-300ºE strip from the example GCM 1981-2000 seasonal climatology shown in figure 5. Colored vertical lines: large-scale features of this profile as defined by the criteria of section 4b(i) [left to right: south mid-latitude maximum, south subtropical minimum, (single) ITCZ maximum, north subtropical minimum, north mid-latitude maximum]. Black horizontal lines: boundaries of the inter-feature precipitation bins to which each point of the profile is assigned for response-recording purposes, according to section 4b(ii).

Figure 7. The percentage **d** of latitudes with significant 21st-century drying trends in P, and the percentage **w** of latitudes with significant 21st-century wetting trends in P, for each precipitation bin of each segment of the example initial P climatology profile shown in figure 6. The bins are arranged in geographic order within each segment: from lowest-P to highest-P going up the bottom rectangle, then from highest-P to lowest-P going up the next rectangle, and so forth. Ordinates with missing data correspond to bins in figure 6 that do not contain any points.

Figure 8. As figure 5, but with the locations of significant pointwise P trends highlighted in red and blue (in the manner of figure 4), and only the particular 10º slice used in figures 6 and 7 outlined in cyan. The correspondence between the feature-relative P response seen along this transect, and its representation in figure 7, is apparent.

Figure 9. For each bin of each segment of the pole-to-pole December-February late-20th-century P climatology profile, and for each single GCM, the percentages **d** and **w** of latitudes classified in that bin for which P significantly declines and increases over the 21st century (1981-2099), averaged over all longitude strips globe-wide for which the P climatology features are defined. At each ordinate, one red (blue) dot represents this average **d** (**w**) for one single GCM (**1 dot = 1 model.**)

Figure 10. [As figure 9, but June-August.] For each bin of each segment of the pole-to-pole June-August late-20th-century P climatology profile, and for each single GCM, the percentages **d** and **w** of latitudes classified in that bin for which P significantly declines and increases over the 21st century (1981-2099), averaged over all longitude strips globe-wide for which the P climatology features are defined. At each ordinate, one red (blue) dot represents this average **d** (**w**) for one single GCM (**1 dot = 1 model.**)

Figure 11. The mean of all twelve plots in the family of figures 9 and 10 [December-February, January-March, … , November-January.]

Figure 12. For each bin of each northern-hemisphere segment of the late-20th-century P-E climatology profile, and for each single GCM, the percentages **d** and **w** of latitudes classified in that bin for which P significantly declines and increases over the 21st century (1981-2099), averaged over all longitude strips globe-wide for which the appropriate P-E climatology features are defined, and then over all twelve three-month seasons, as in figure 11. At each ordinate, one red (blue) dot represents this average **d** (**w**) for one single GCM (**1 dot = 1 model.**) Left panel: using only the profile segments with the default P-E feature configuration. Right panel: using only the P-E profile segments associated with a positive north subtropical minimum, as opposed to the default negative minimum.

Figure 13. Left panel: identical to figure 12. Right top panel: using only the P-E profile segments with some negative P-E values poleward of the north mid-latitude maximum, as opposed to the default all-positive values. Right bottom panel: using only the P-E profile segments associated with a negative north ITCZ maximum, as opposed to the default positive maximum.

Figure 14. [As figure 12, but for the southern hemisphere.] South (toward the pole) is plotted *up* for convenient comparison with figure 12. For each bin of each southern-hemisphere segment of the late-20th-century P-E climatology profile, and for each single GCM, the percentages **d** and **w** of latitudes classified in that bin for which P significantly declines and increases over the 21st century (1981-2099), averaged over all longitude strips globe-wide for which the appropriate P-E climatology features are defined, and then over all twelve three-month seasons, as in figure 11. At each ordinate, one red (blue) dot represents this average **d** (**w**) for one single GCM (**1 dot = 1 model.**) Left panel: using only the profile segments with the default P-E feature configuration. Right panel: using only the P-E profile segments associated with a positive south subtropical minimum, as opposed to the default negative minimum.

Figure 15. [As figure 13, but for the southern hemisphere.] South (toward the pole) is plotted *up* for convenient comparison with figure 13. Left panel: identical to figure 14. Right top panel: using only the P-E profile segments with some negative P-E values poleward of the south mid-latitude maximum, as opposed to the default all-positive values. Right bottom panel: using only the P-E profile segments associated with a negative south ITCZ maximum, as opposed to the default positive maximum.

Figure 16. For each bin of each segment of the pole-to-pole December-February late-20th-century P climatology profile in each 10°-longitude zonal mean, the percentage **d** of latitudes classified in that bin for which P significantly declines over the 21st century (1981-2099), averaged over all GCMs for which the P climatology features are defined at that longitude. Hemisphere-longitudes for which less than 50% of the GCMs have these features defined, and thus less than 50% of the GCMs contribute to the plotted profiles, are struck through in magenta as a warning.

Figure 17. [As figure 16, but for **w**.] For each bin of each segment of the pole-to-pole December-February late-20th-century P climatology profile in each 10°-longitude zonal mean, the percentage **w** of latitudes classified in that bin for which P significantly increases over the 21st century (1981-2099), averaged over all GCMs for which the P climatology features are defined at that longitude. Hemisphere-longitudes for which less than 50% of the GCMs have these features defined, and thus less than 50% of the GCMs contribute to the plotted profiles, are struck through in magenta as a warning.

Figure 18. [As figure 16, but June-August.] For each bin of each segment of the pole-to-

pole June-August late-20th-century P climatology profile in each 10°-longitude zonal mean, the percentage **d** of latitudes classified in that bin for which P significantly declines over the 21st century (1981-2099), averaged over all GCMs for which the P climatology features are defined at that longitude. Hemisphere-longitudes for which less than 50% of the GCMs have these features defined, and thus less than 50% of the GCMs contribute to the plotted profiles, are struck through in magenta as a warning.

Figure 19. [As figure 17, but June-August.] For each bin of each segment of the pole-to-pole June-August late-20th-century P climatology profile in each 10°-longitude zonal mean, the percentage **w** of latitudes classified in that bin for which P significantly increases over the 21st century (1981-2099), averaged over all GCMs for which the P climatology features are defined at that longitude. Hemisphere-longitudes for which less than 50% of the GCMs have these features defined, and thus less than 50% of the GCMs contribute to the plotted profiles, are struck through in magenta as a warning.

Appendix: Figures (with captions)

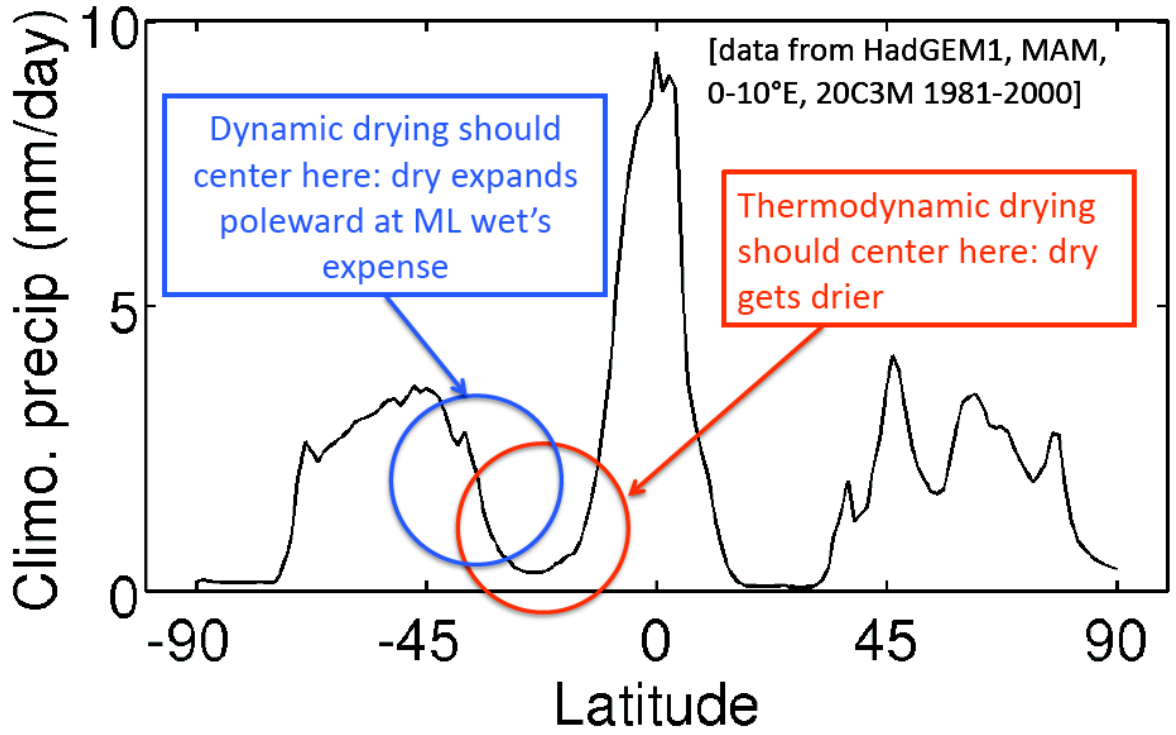

Figure 1. Conceptual model for inferring the dynamic vs. thermodynamic nature of simulated subtropical precipitation reductions. The simulated late 20th century precipitation climatology for a particular model, time of year, and longitude band is plotted, but we could ask this question for any model, at any time of year, and in any longitude where there is a distinct subtropical minimum and mid-latitude maximum. We could have also used the climatology of precipitation minus evaporation.

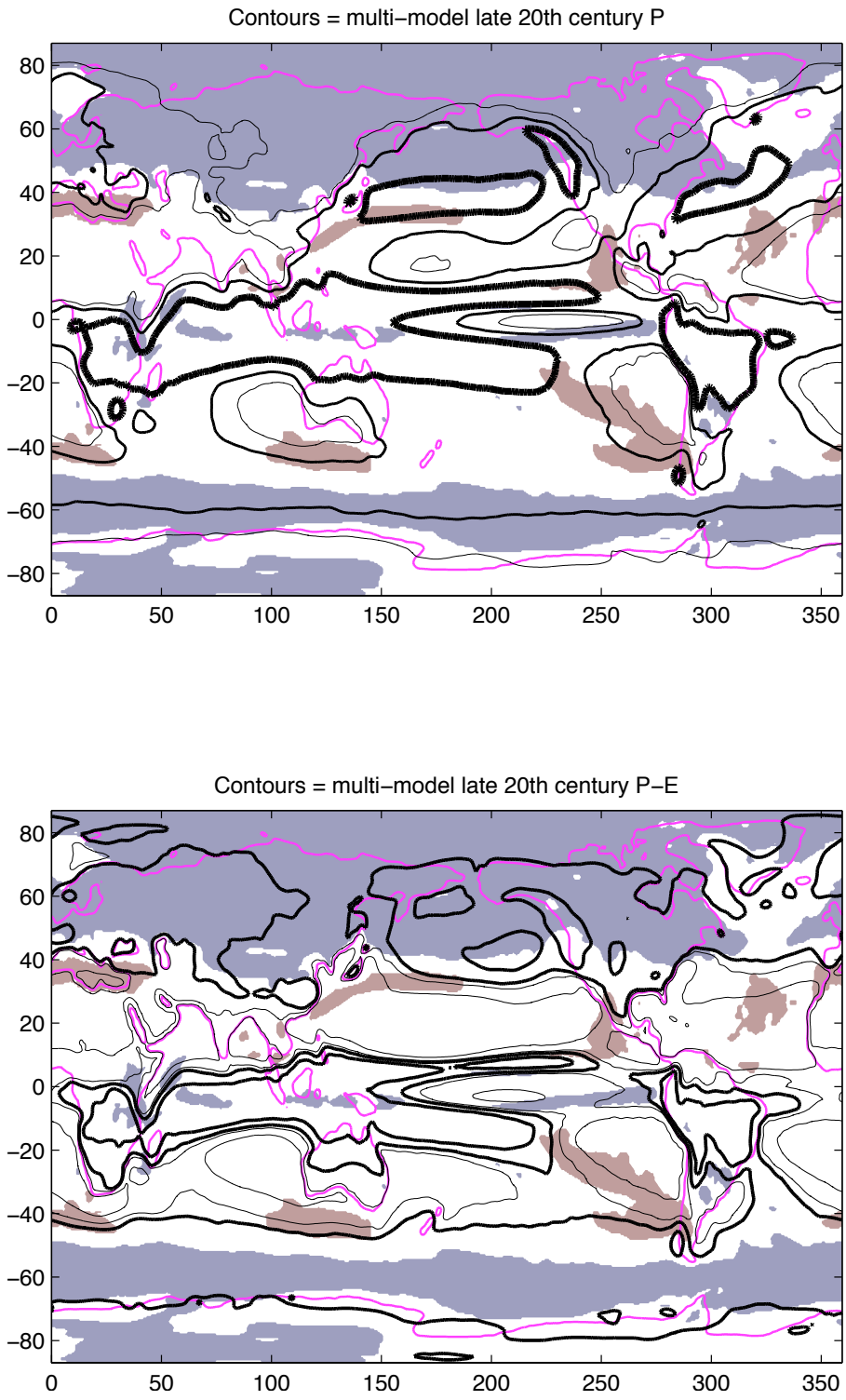

Figure 2. All data December-February only. Black contours: 1981-2000 multi-model climatological precipitation (top panel; 1, 2, 5 mm/day lightest to boldest) and precipitation minus evaporation (bottom panel; -2.5, -0.5 mm/day light; +0.5, +2.5 mm/day bold; 0 contour not shown). Colors: locations of robust multi-model 21st century precipitation decreases (red) and increases (blue); colors are reproduced in both panels.

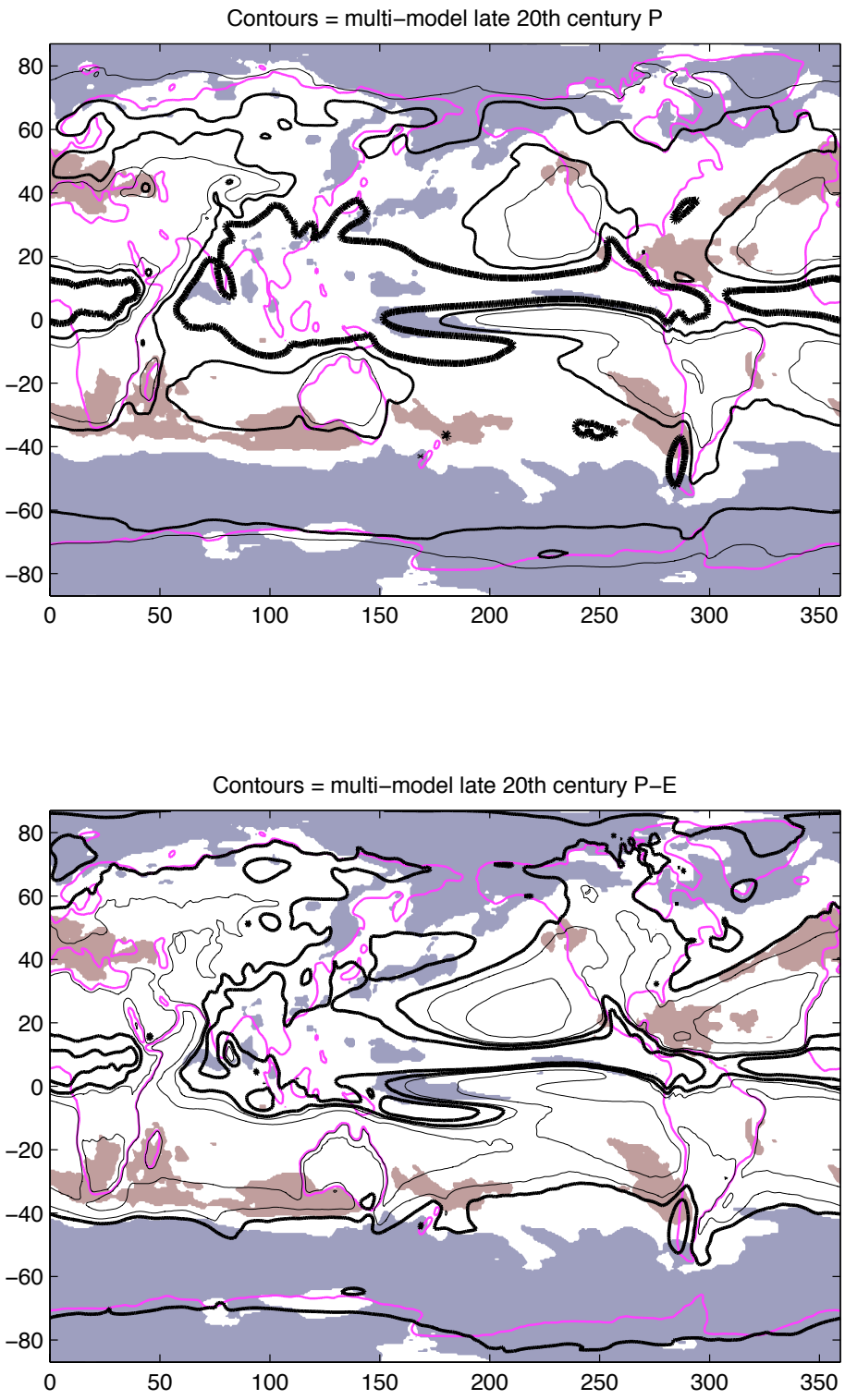

Figure 3. As figure 2, but all data June-August only. Black contours: 1981-2000 multi-model climatological precipitation (top panel; 1, 2, 5 mm/day lightest to boldest) and precipitation minus evaporation (bottom panel; -2.5, -0.5 mm/day light; +0.5, +2.5 mm/day bold; 0 contour not shown). Colors: locations of robust multi-model 21st century precipitation decreases (red) and increases (blue); colors are reproduced in both panels.

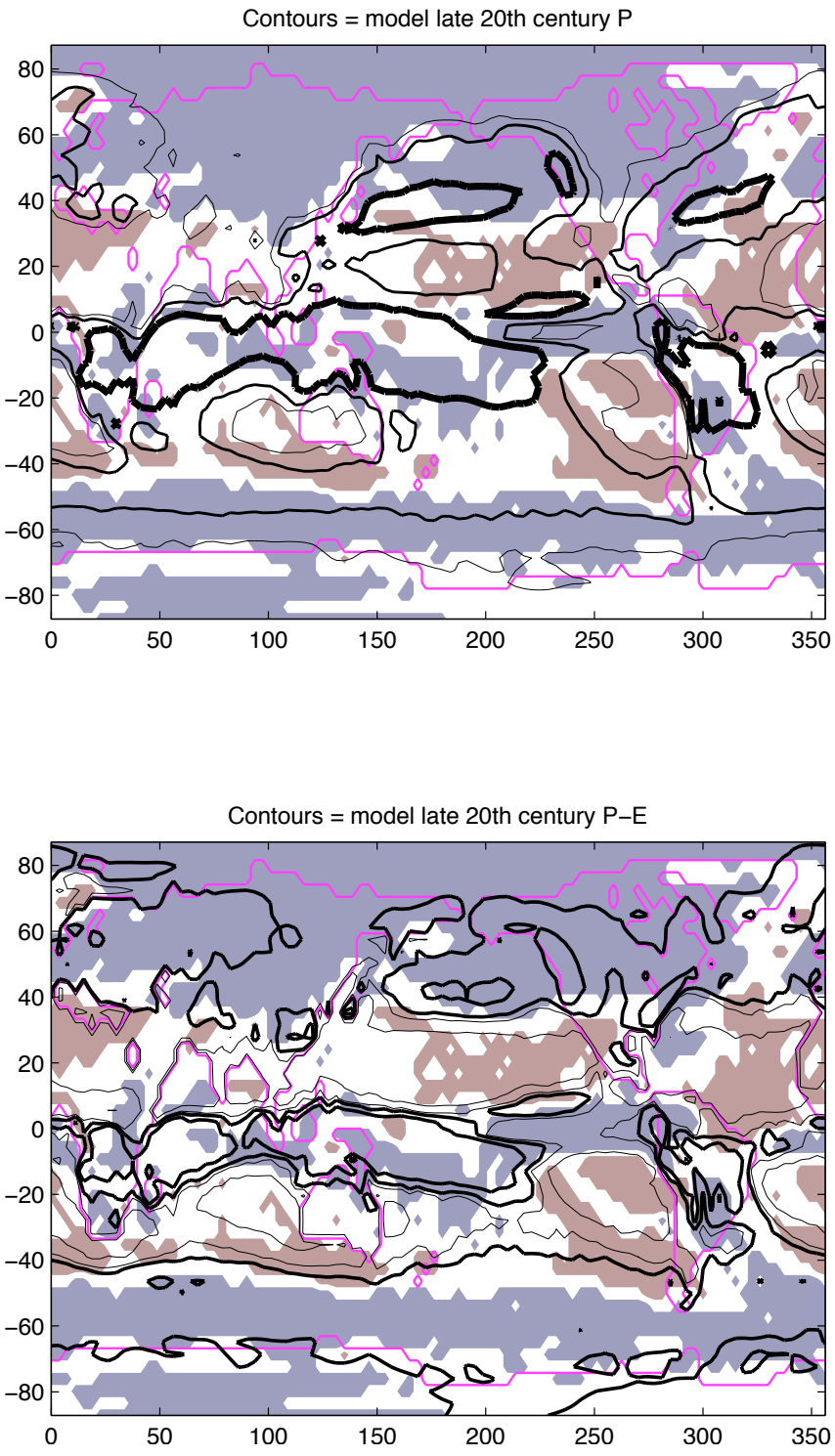

Figure 4. All data December-February only, and for the single GCM "cccma" only. Black contours: 1981-2000 single-model climatological precipitation (top panel; 1, 2, 5 mm/day lightest to boldest) and precipitation minus evaporation (bottom panel; -2.5, -0.5 mm/day light; +0.5, +2.5 mm/day bold; 0 contour not shown). Colors: locations of 95%-significant single-model precipitation decreases (red) and increases (blue) using the 1981-2099 linear trends; colors are reproduced in both panels.

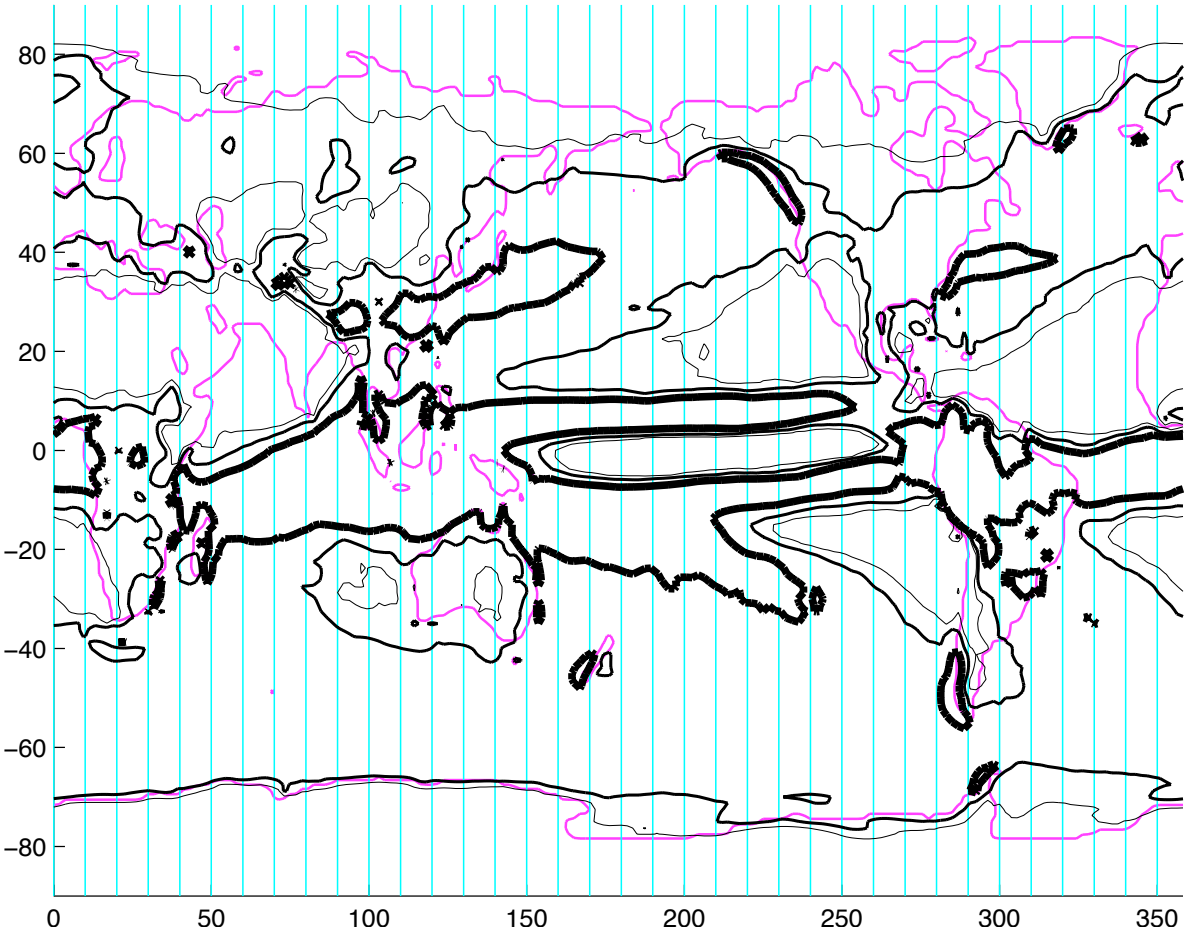

Figure 5. Example of the slicing of a single-GCM precipitation climatology (black contours) into thirty-six 10º-longitude-wide strips over which zonal means will be taken; the latitudes of the ITCZ maxim(a), subtropical minima and mid-latitude maxima can now be separately identified for each strip that possesses them, using the criteria of section 4b(i). The example climatology shown is that of model "hadgem1", 1981-2000, for the March-May season.

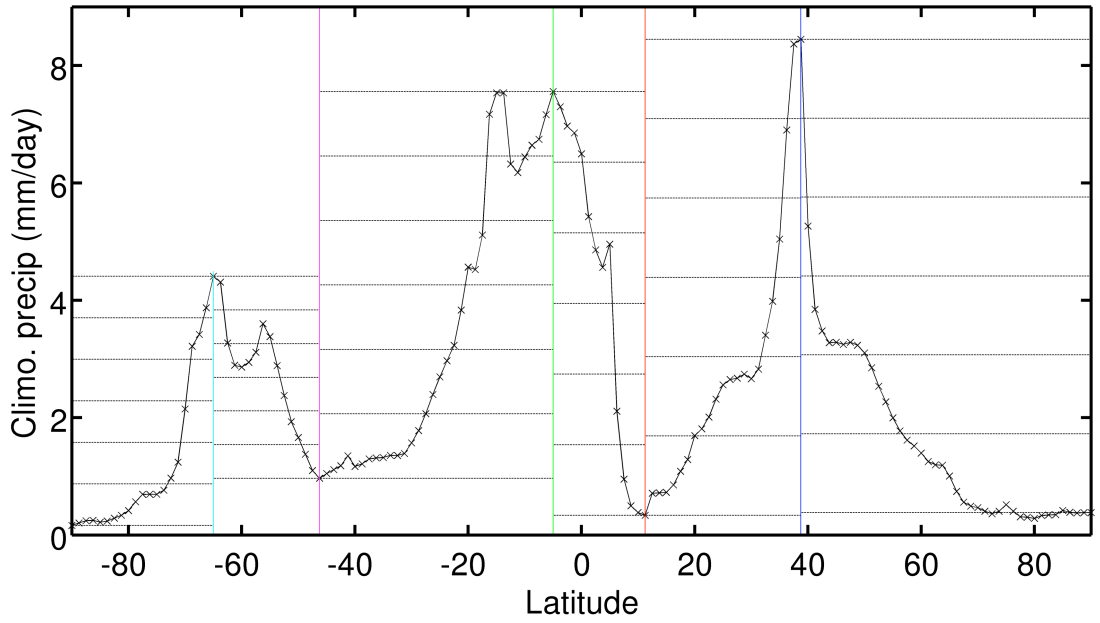

Figure 6. Black curve: zonal-average precipitation vs. latitude profile for the 290º-300ºE strip from the example GCM 1981-2000 seasonal climatology shown in figure 5. Colored vertical lines: large-scale features of this profile as defined by the criteria of section 4b(i) [left to right: south mid-latitude maximum, south subtropical minimum, (single) ITCZ maximum, north subtropical minimum, north mid-latitude maximum]. Black horizontal lines: boundaries of the inter-feature precipitation bins to which each point of the profile is assigned for response-recording purposes, according to section 4b(ii).

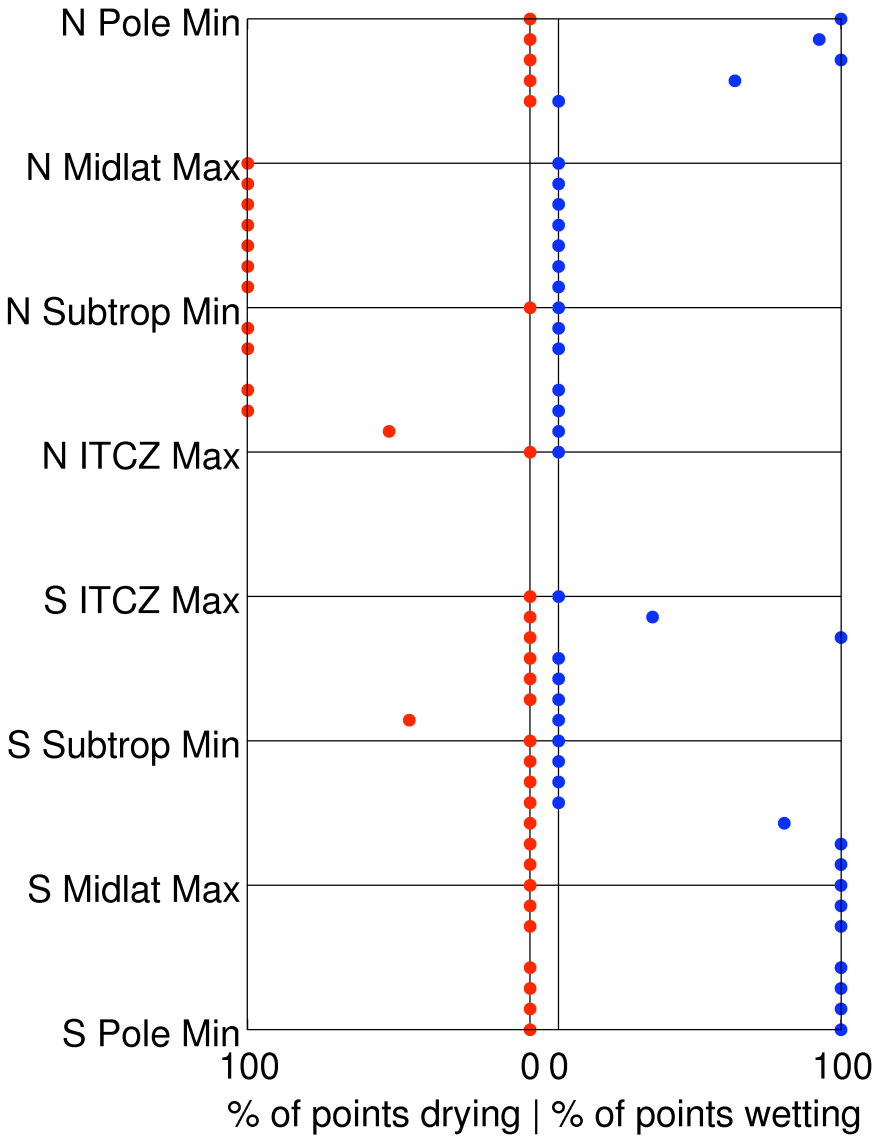

Figure 7. The percentage of latitudes **d** with significant 21st-century drying trends in P, and the percentage of latitudes **w** with significant 21st-century wetting trends in P, for each precipitation bin of each segment of the example initial P climatology profile shown in figure 6. The bins are arranged in geographic order within each segment: from lowest-P to highest-P going up the bottom rectangle, then from highest-P to lowest-P going up the next rectangle, and so forth. Ordinates with missing data correspond to bins in figure 6 that do not contain any points.

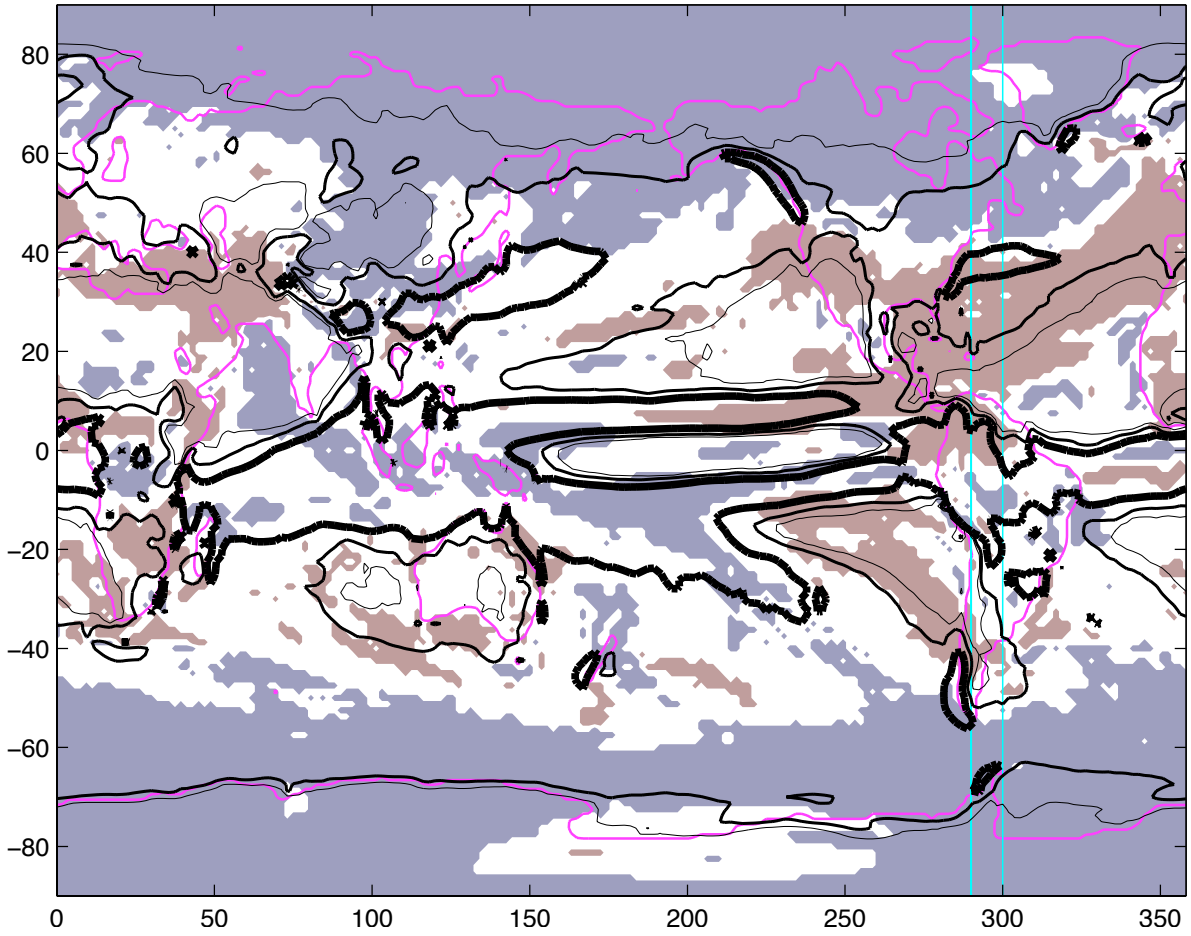

Figure 8. As figure 5, but with the locations of significant pointwise P trends highlighted in red and blue (in the manner of figure 4), and only the particular 10º slice used in figures 6 and 7 outlined in cyan. The correspondence between the feature-relative P response seen along this transect, and its representation in figure 7, is apparent.

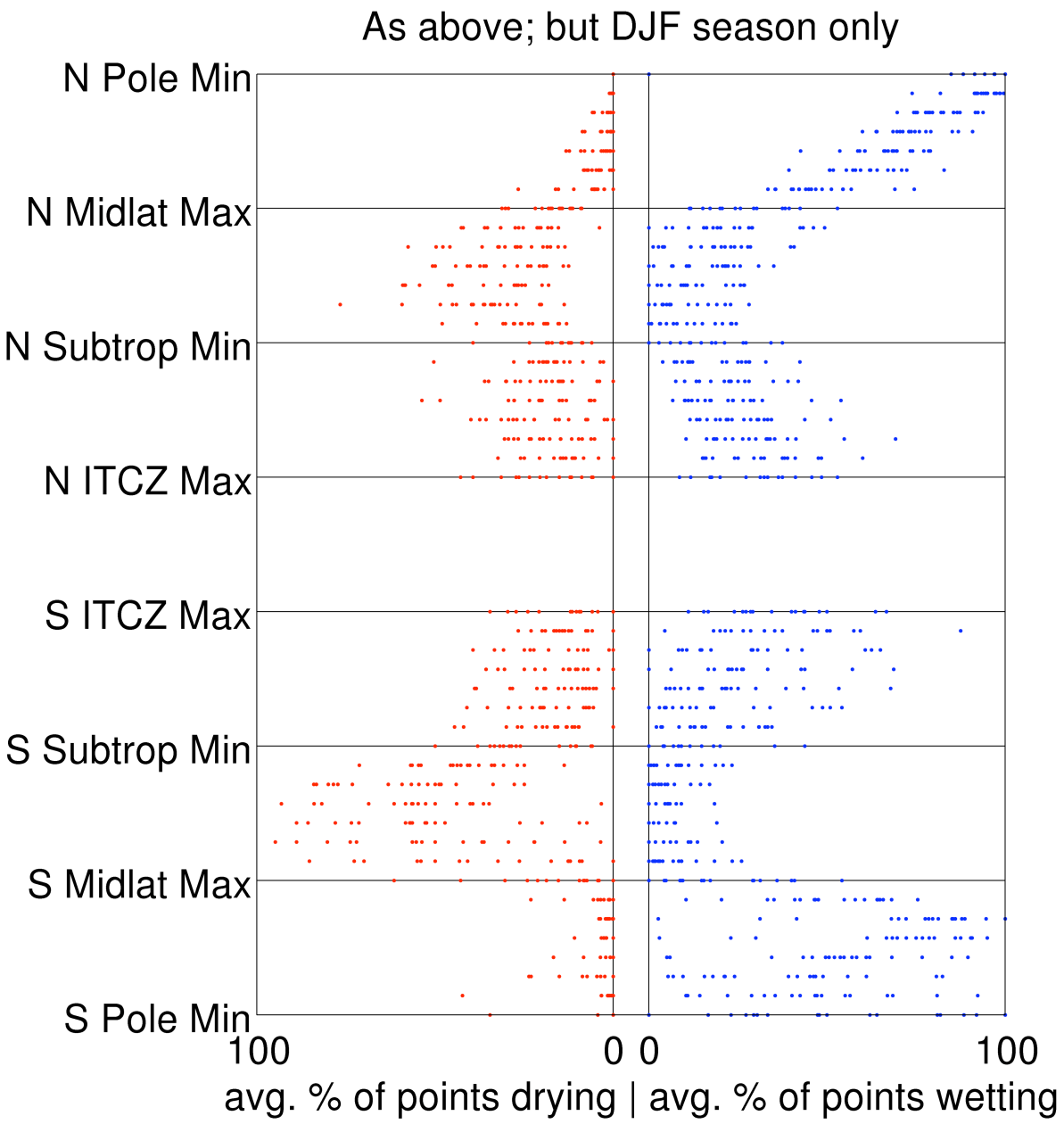

Figure 9. For each bin of each segment of the pole-to-pole December-February late-20th-century P climatology profile, and for each single GCM, the percentages **d** and **w** of latitudes classified in that bin for which P significantly declines and increases over the 21st century (1981-2099), averaged over all longitude strips globe-wide for which the P climatology features are defined. At each ordinate, one red (blue) dot represents this average **d** (**w**) for one single GCM (**1 dot = 1 model.**)

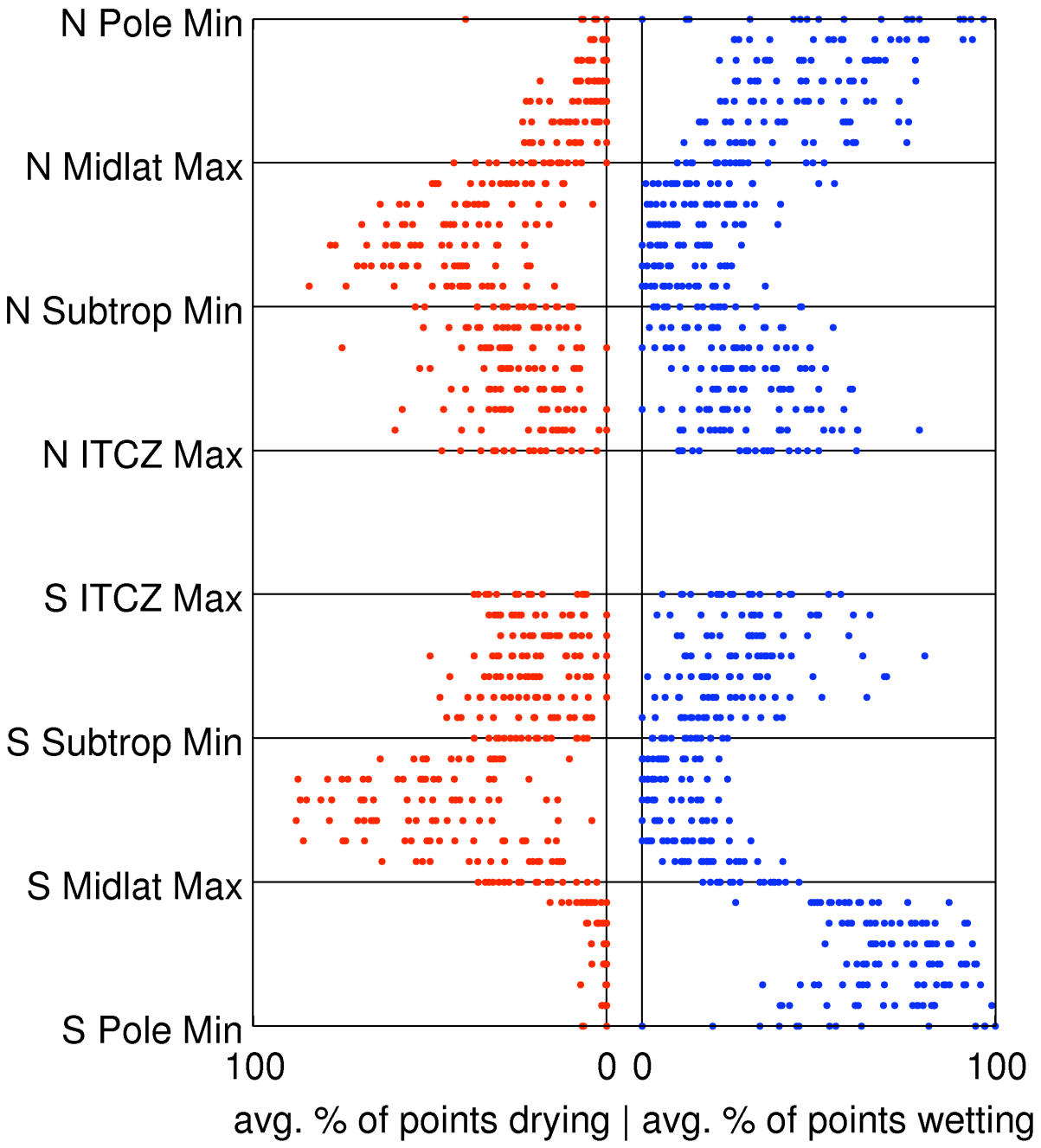

Figure 10. [As figure 9, but June-August.] For each bin of each segment of the pole-to-pole June-August late-20th-century P climatology profile, and for each single GCM, the percentages **d** and **w** of latitudes classified in that bin for which P significantly declines and increases over the 21st century (1981-2099), averaged over all longitude strips globe-wide for which the P climatology features are defined. At each ordinate, one red (blue) dot represents this average **d** (**w**) for one single GCM (**1 dot = 1 model.**)

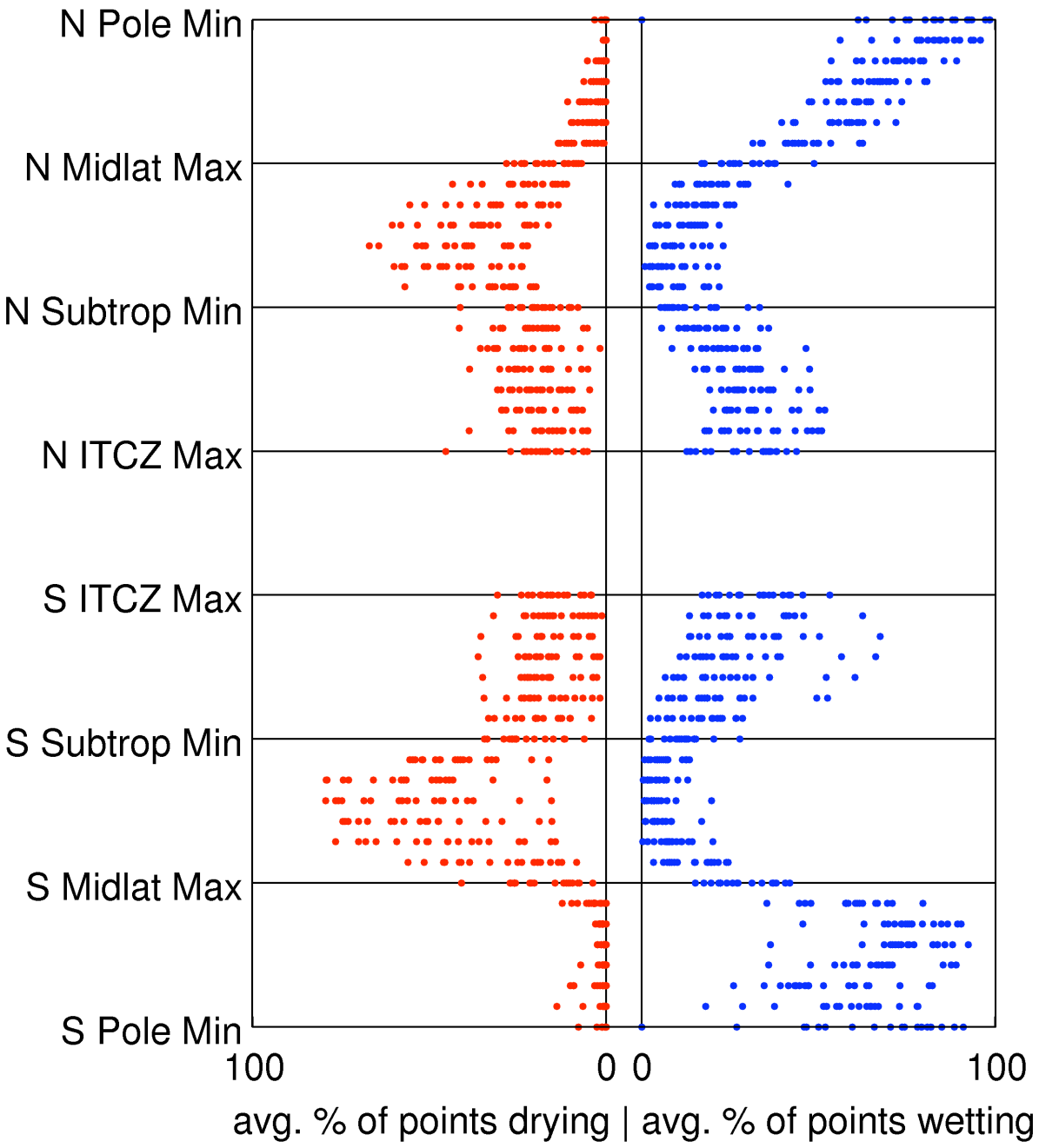

Figure 11. The mean of all twelve plots in the family of figures 9 and 10 [December-February, January-March, … , November-January.]

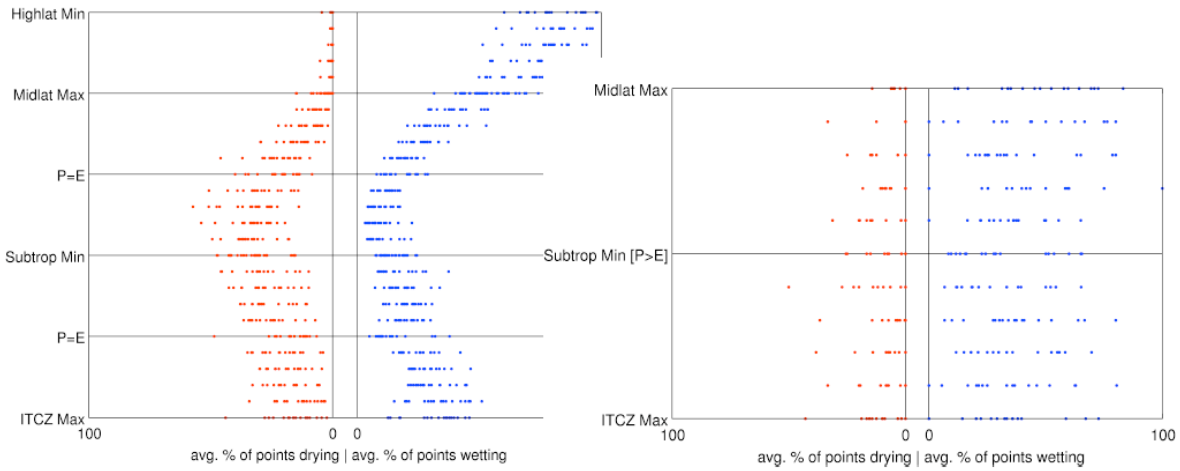

Figure 12. For each bin of each northern-hemisphere segment of the late-20th-century P-E climatology profile, and for each single GCM, the percentages **d** and **w** of latitudes classified in that bin for which P significantly declines and increases over the 21st century (1981-2099), averaged over all longitude strips globe-wide for which the appropriate P-E climatology features are defined, and then over all twelve three-month seasons, as in figure 11. At each ordinate, one red (blue) dot represents this average **d** (**w**) for one single GCM (**1 dot = 1 model.**) Left panel: using only the profile segments with the default P-E feature configuration. Right panel: using only the P-E profile segments associated with a positive north subtropical minimum, as opposed to the default negative minimum.

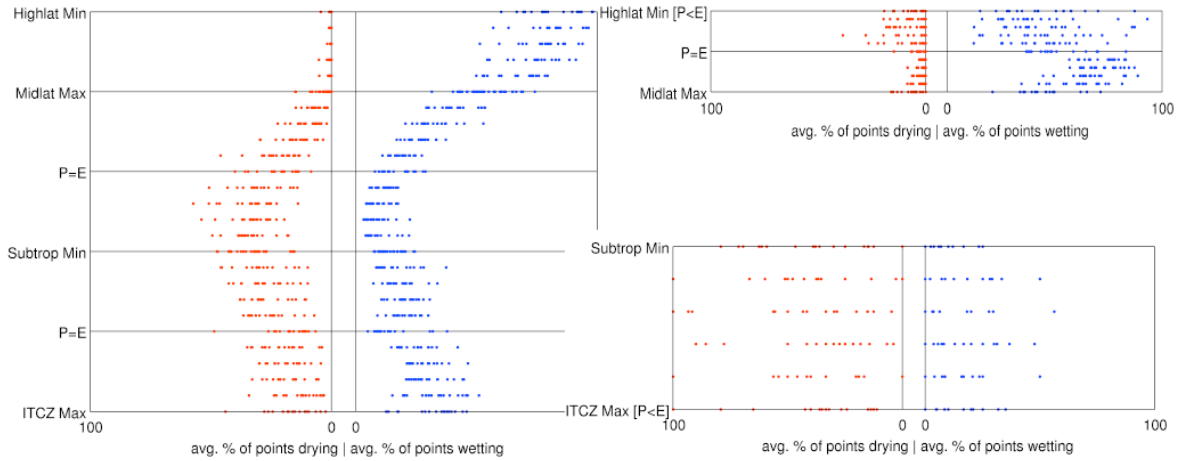

Figure 13. Left panel: identical to figure 12. Right top panel: using only the P-E profile segments with some negative P-E values poleward of the north mid-latitude maximum, as opposed to the default all-positive values. Right bottom panel: using only the P-E profile segments associated with a negative north ITCZ maximum, as opposed to the default positive maximum.

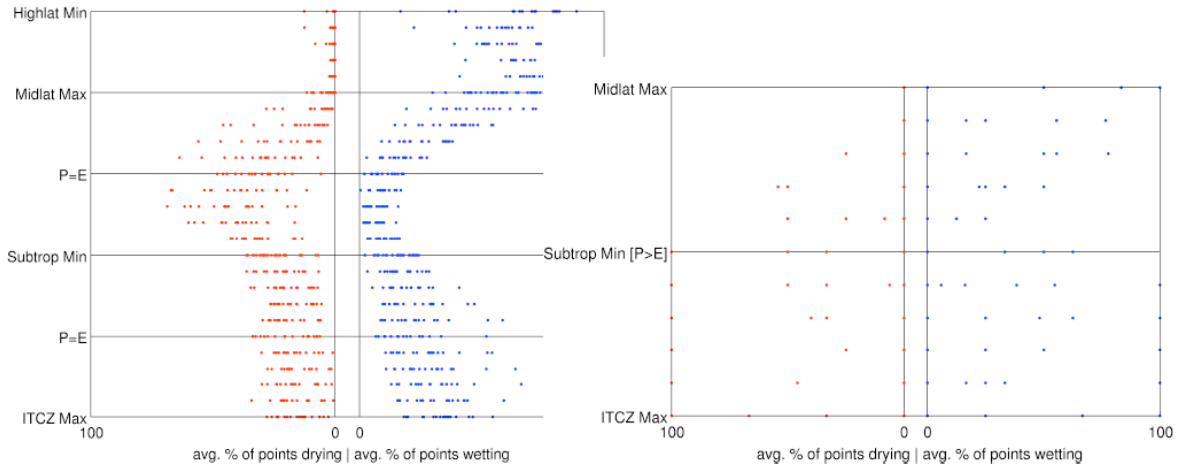

Figure 14. [As figure 12, but for the southern hemisphere.] South (toward the pole) is plotted *up* for convenient comparison with figure 12. For each bin of each southern-hemisphere segment of the late-20th-century P-E climatology profile, and for each single GCM, the percentages **d** and **w** of latitudes classified in that bin for which P significantly declines and increases over the 21st century (1981-2099), averaged over all longitude strips globe-wide for which the appropriate P-E climatology features are defined, and then over all twelve three-month seasons, as in figure 11. At each ordinate, one red (blue) dot represents this average **d** (**w**) for one single GCM (**1 dot = 1 model.**) Left panel: using only the profile segments with the default P-E feature configuration. Right panel: using only the P-E profile segments associated with a positive south subtropical minimum, as opposed to the default negative minimum.

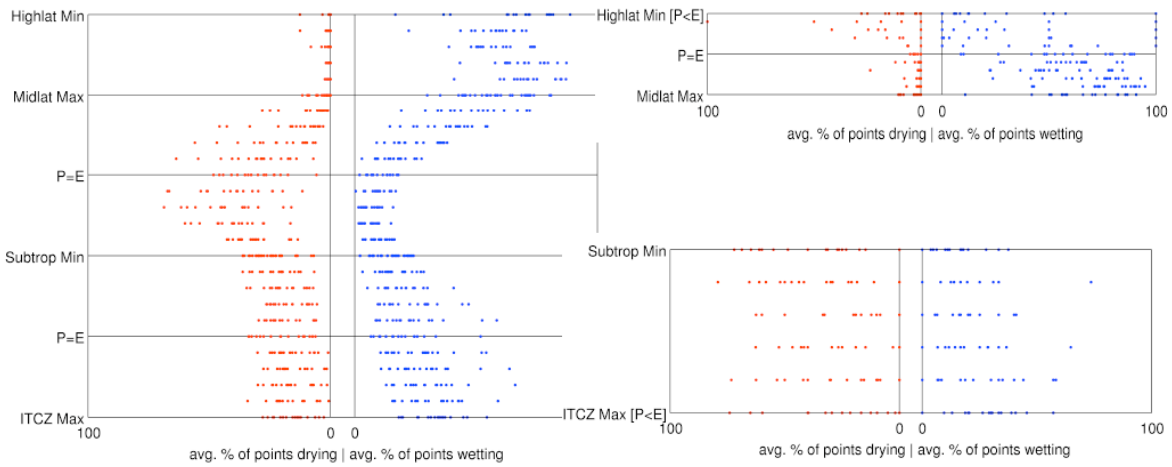

Figure 15. [As figure 13, but for the southern hemisphere.] South (toward the pole) is plotted *up* for convenient comparison with figure 13. Left panel: identical to figure 14. Right top panel: using only the P-E profile segments with some negative P-E values poleward of the south mid-latitude maximum, as opposed to the default all-positive values. Right bottom panel: using only the P-E profile segments associated with a negative south ITCZ maximum, as opposed to the default positive maximum.

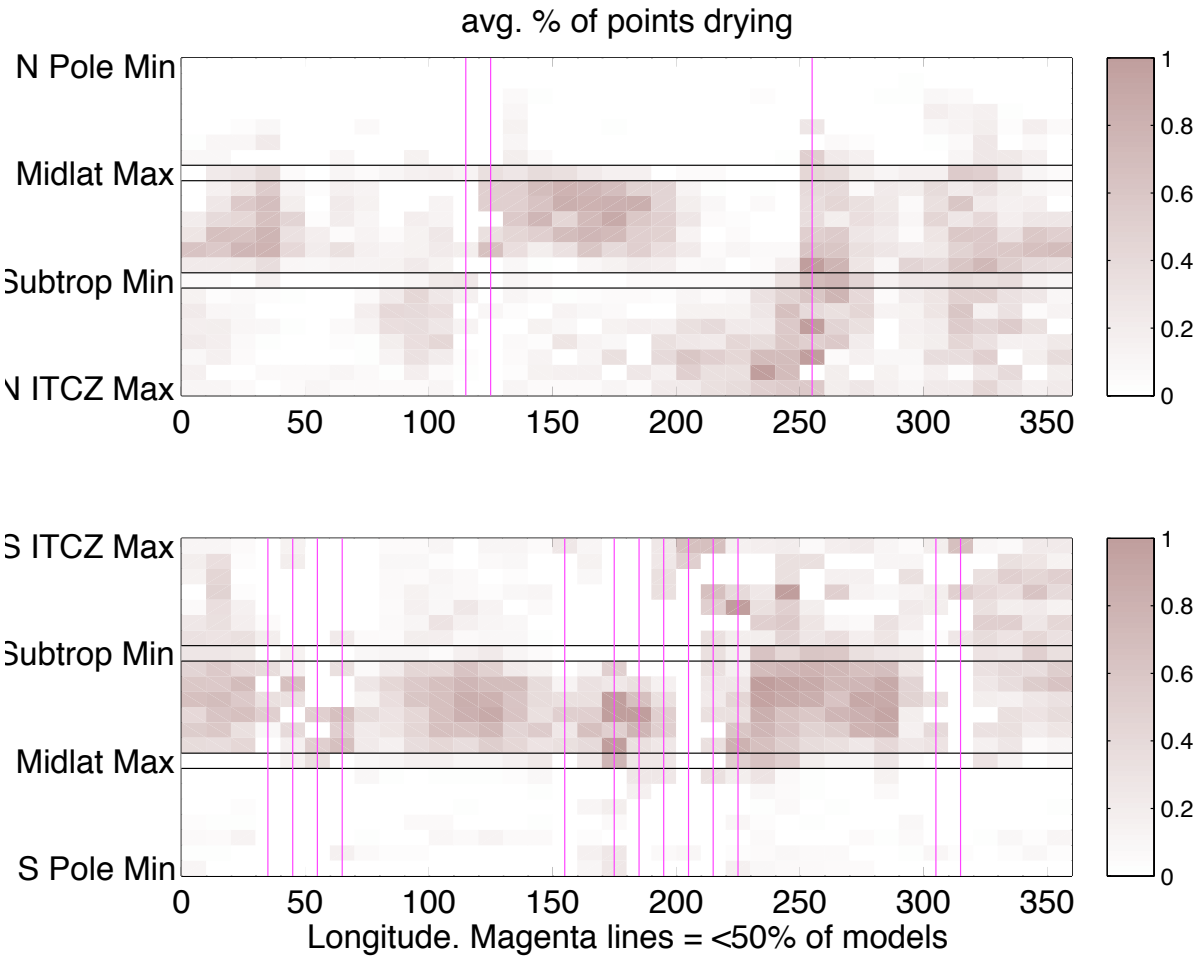

Figure 16. For each bin of each segment of the pole-to-pole December-February late-20th-century P climatology profile in each 10°-longitude zonal mean, the percentage **d** of latitudes classified in that bin for which P significantly declines over the 21st century (1981-2099), averaged over all GCMs for which the P climatology features are defined at that longitude. Hemisphere-longitudes for which less than 50% of the GCMs have these features defined, and thus less than 50% of the GCMs contribute to the plotted profiles, are struck through in magenta as a warning.

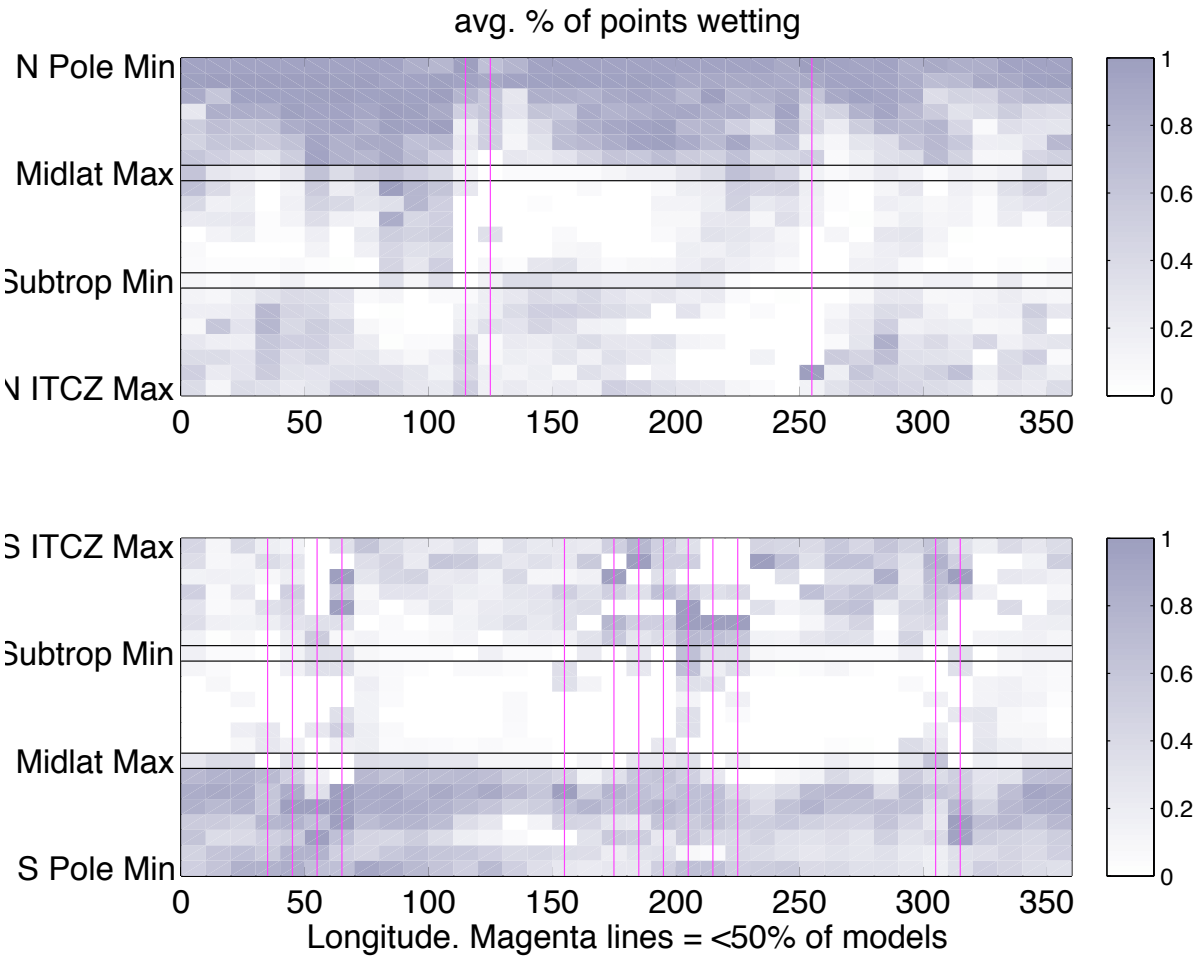

Figure 17. [As figure 16, but for **w**.] For each bin of each segment of the pole-to-pole December-February late-20th-century P climatology profile in each 10°-longitude zonal mean, the percentage **w** of latitudes classified in that bin for which P significantly increases over the 21st century (1981-2099), averaged over all GCMs for which the P climatology features are defined at that longitude. Hemisphere-longitudes for which less than 50% of the GCMs have these features defined, and thus less than 50% of the GCMs contribute to the plotted profiles, are struck through in magenta as a warning.

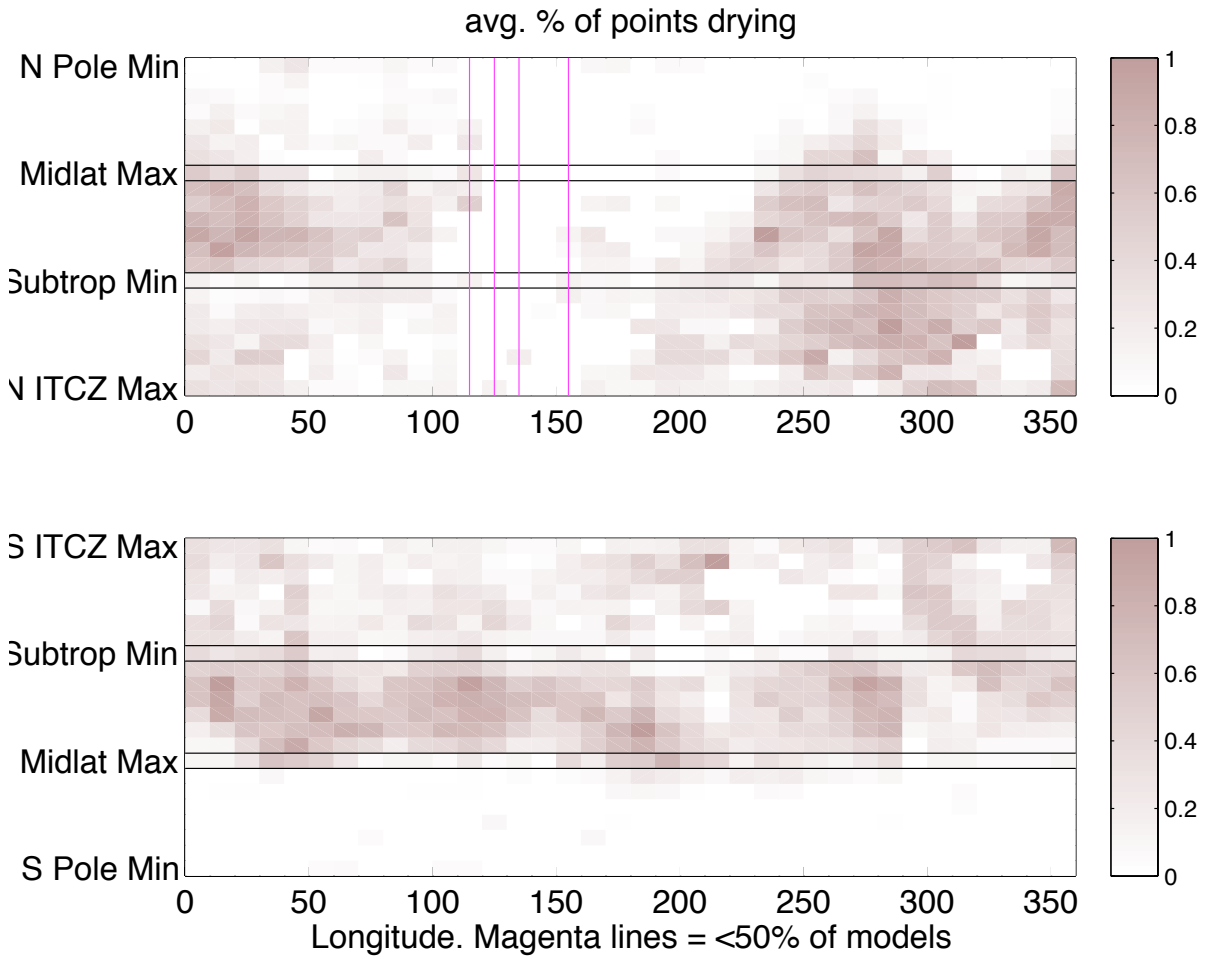

Figure 18. [As figure 16, but June-August.] For each bin of each segment of the pole-to-pole June-August late-20th-century P climatology profile in each 10°-longitude zonal mean, the percentage **d** of latitudes classified in that bin for which P significantly declines over the 21st century (1981-2099), averaged over all GCMs for which the P climatology features are defined at that longitude. Hemisphere-longitudes for which less than 50% of the GCMs have these features defined, and thus less than 50% of the GCMs contribute to the plotted profiles, are struck through in magenta as a warning.

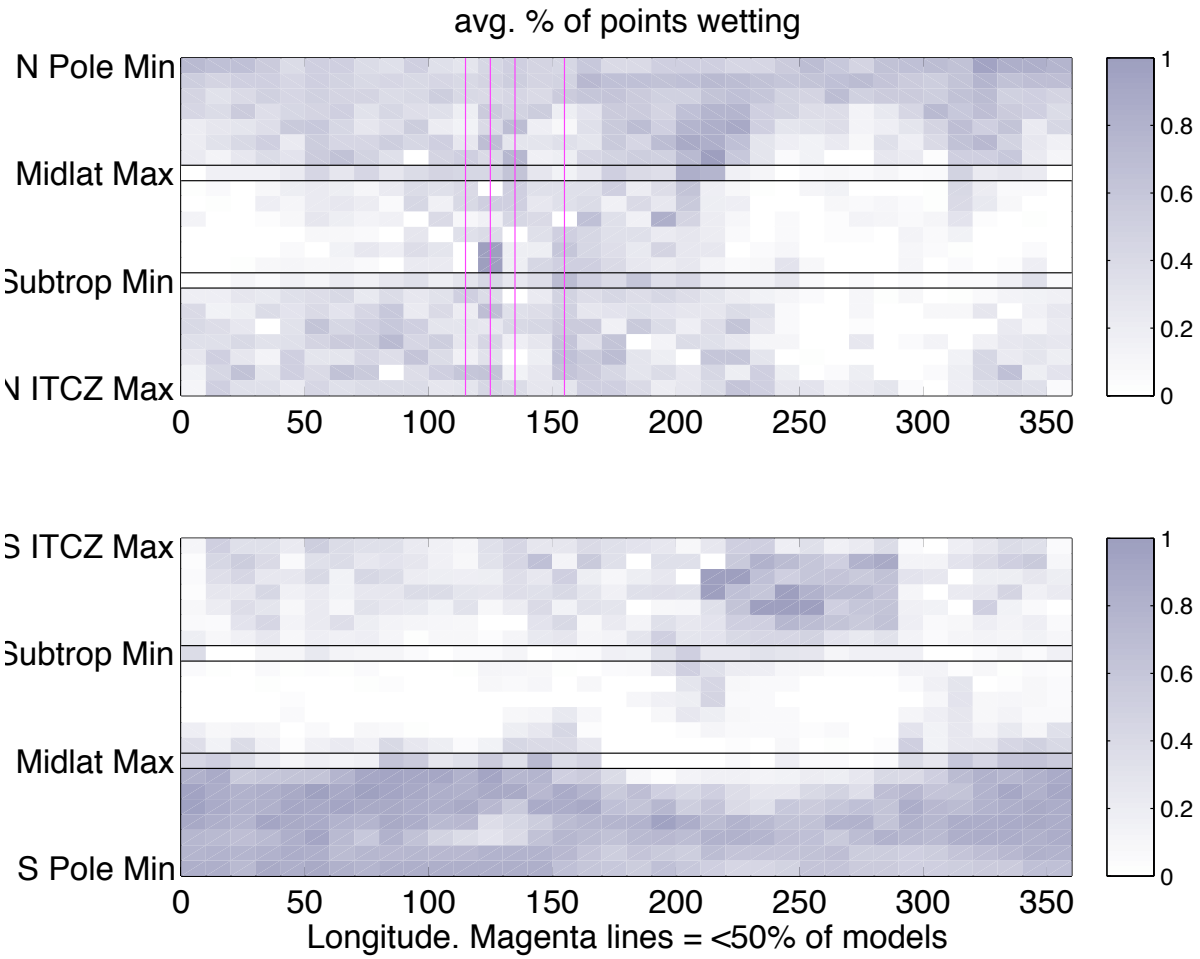

Figure 19. [As figure 17, but June-August.] For each bin of each segment of the pole-to-pole June-August late-20th-century P climatology profile in each 10°-longitude zonal mean, the percentage **w** of latitudes classified in that bin for which P significantly increases over the 21st century (1981-2099), averaged over all GCMs for which the P climatology features are defined at that longitude. Hemisphere-longitudes for which less than 50% of the GCMs have these features defined, and thus less than 50% of the GCMs contribute to the plotted profiles, are struck through in magenta as a warning.